

Importance of wave age and resonance in storm surges: The case Xynthia, Bay of Biscay

Xavier Bertin ^{a,*}, Nicolas Bruneau ^{b,1}, Jean-François Breilh ^a, André B. Fortunato ^b, Mikhail Karpytchev ^a

^a UMR 6250 LIENSs CNRS-Université de La Rochelle, Institut du Littoral et de l'Environnement, 2 rue Olympe de Gouges, 17000 La Rochelle, France

^b Estuaries and Coastal Zones Division, National Laboratory of Civil Engineering, Av. do Brasil, 101, 1700-066 Lisbon, Portugal

ARTICLE INFO

Article history:

Received 8 August 2011

Received in revised form 21 September 2011

Accepted 2 November 2011

Available online 25 November 2011

Keywords:

Xynthia
Storm surge
Numerical model
Resonance
Wave age
Friction velocity

ABSTRACT

This study aims to hindcast and analyze the storm surge associated with Xynthia, a mid-latitude depression that severely hit the French central part of the Bay of Biscay on the 27–28th of February 2010. The main losses in human lives and damages were caused by the associated storm surge, which locally exceeded 1.5 m and peaked at the same time as a high spring tide, causing the flooding of low-lying coasts. A new storm surge modeling system was developed, based on the unstructured-grid circulation model SELFE and the spectral wave model WaveWatchIII. The modeling system was implemented over the North-East Atlantic Ocean and resulted in tidal and wave predictions with errors of the order of 3% and 15%, respectively. The storm surge associated with Xynthia was also well predicted along the Bay of Biscay, with only a slight underestimation of the surge peak by 3–8%. Numerical experiments were then performed to analyze the physical processes controlling the development of the storm surge and revealed firstly that the wind caused most of the water level anomaly through an Ekman setup process. The comparison between a wave-dependant and a quadratic parameterization to compute wind stress showed that the storm surge was strongly amplified by the presence of steep and young wind-waves, related to their rapid development in the restricted fetch of the Bay of Biscay. In the central part of the Bay of Biscay, both observed and predicted water level anomalies at landfall displayed ~6 h oscillations, with amplitudes of up to 0.2 m (10–20% of the surge peak). An analytical shelf resonance model and numerical experiments demonstrated that the period of the observed oscillations corresponds to the resonant mode of the continental shelf in the central part of the Bay of Biscay. It is concluded that these oscillations originate from the interactions between the water level perturbation and the continental shelf and this phenomenon is expected to be relevant at other places along the world's coastlines.

© 2011 Elsevier Ltd. All rights reserved.

1. Introduction

Storm surges correspond to abnormal variations in the ocean free-surface driven by atmospheric forcing associated with extra-tropical storms or tropical hurricanes and typhoons (Flather, 2001). At low-lying coasts, the largest damages are usually associated with the storm surge and the subsequent flooding rather than direct wind effects, particularly if the surge coincides with high tides. According to the governing shallow water equations (SWE), written in non conservative form, the wind stress is divided by the water depth, which causes the wind effect to be dominant over atmospheric pressure gradients in shallow waters. Low-lying coasts bordered by extensive continental shelves and exposed to the regular passing of hurricanes and storms are thus particularly vulnerable to storm surges and coastal flooding. The Bay of Bengal

combines these settings and is the region in the world where the deadliest hurricane-induced surges were reported. Thus, on the 12th of November 1970, the Bhola tropical cyclone struck and devastated Bangladesh and India's West Bengal, killing between 300,000 and 500,000 lives (Das, 1972; Flather, 2001). More recently, the tropical cyclone Nargis flooded the low-lying Irrawaddy delta (Birmanya, now Myanmar) in early May 2008 and killed over 130,000 people (Wolf, 2009). Also very vulnerable is the Gulf of Mexico, which combines a large continental shelf, shallow back-barrier and delta coastal morphologies, and the regular passing of tropical cyclones in late summer and autumn. Hurricane Katrina was the sixth-strongest Atlantic hurricane ever reported and was the costliest and the third deadliest in the history of the United States (84 billions \$ damage and 1500 deaths; Blake, 2007). Atmospheric pressure reached 920 mbar at landfall and maximum wind speed up to 70 m s^{-1} , which produced significant wave heights larger than 16 m and a storm surge exceeding 8 m in several locations along the Mississippi coastlines (Dietrich et al., 2010; Blake, 2007). To a slighter degree, North-Western Europe is also submitted to

* Corresponding author. Tel.: +33 546507636; fax: +33 546458274.

E-mail address: xbertin@univ-lr.fr (X. Bertin).

¹ Both authors contributed equally to this work.

storm surge and coastal flooding risks. Actually, this region of the world is located on the path of mid-latitude depressions and combines low-lying barrier islands and estuaries surrounded by large continental shelves. Thus, on the 31th of January 1953, a severe storm over the North Sea induced a surge that exceeded 3.0 m along the coast of Netherlands and peaked at the time of spring-tide high water. The subsequent high water level caused the breaching of 150 sea-dykes and the flooding of low-lying regions inhabited by around 750,000 people, 1836 of whom passed away tragically (Gerritsen, 2005; Wolf and Flather, 2005). On the other side of England, the Irish Sea is also exposed to large storm surges, despite being a small sea, not fully exposed to the Atlantic Ocean. The strong winds due to mid-latitude depressions blowing over water depths of the order of 40 m produce storm surges that can attain up to 2.5 m (Brown and Wolf, 2009; Brown et al., 2010). Due to sea-level rise and the potential increase in storminess resulting from climate change, extreme coastal flooding events are likely to increase in the future (Brown et al., 2010) while the population in coastal zones is expected to increase (IPCC, 2007). In this context, the accurate forecast of storm surges and subsequent coastal flooding appear highly priority for numerous socio-economical issues.

Storm surges are being investigated using numerical models since the mid nineteen sixties (Jelesnianski, 1965, 1966; Miyazaki, 1965; Miyazaki and Okada, 1975). Since these pioneering studies, the better understanding of oceanic physical processes together with an exponential growth of computational capacities have permitted the development of sophisticated modeling systems capable of efficiently simulating storm surges with a high resolution over large geographical extensions (e.g. Bunya et al., 2010; Dietrich et al., 2010). Among the abundant literature available on the subject, a common procedure consists of performing a hindcast of a relevant hurricane, and then analysing the physical processes responsible for the associated surge. Thus, several studies showed that, in shallow water, wind stress was dominant over the well known “inverse barometer effect” (Doodson, 1924) caused by atmospheric pressure gradients (Jones and Davies, 2007; Rego and Li, 2010). Under steady state and in deep water, the alongshore component of wind stress drives an “Ekman setup” (Shen and Gong, 2009; Kennedy et al., 2011) at the coast located to the right-side of the wind (in the northern hemisphere), although the cross-shore component of wind stress becomes dominant in shallower water due to the increase in bottom stress (Weisberg and Zheng, 2006; Rego and Li, 2010). Kennedy et al. (2011) reported a large water level anomaly along the coasts of Louisiana and Texas (USA) 12–24 h before the landfall of Hurricane Ike (2008) and attributed the origin of these forerunners anomalies to such an Ekman setup. Tide-surge interaction was also shown to be relevant for the adequate prediction of storm surges (Proudman, 1957; Wolf, 2009; Rego and Li, 2010; Zhang et al., 2010). According to Wolf (1981), shallow water effects (i.e. non-linear terms containing the total water depth in SWE) are dominant for tidal ranges larger than 3 m and water depths below 10 m. For larger depths (50 m) with significant tidal currents, Zhang et al. (2010) showed in the Taiwan Strait that the dominant effect in tide-surge interactions was non-linear bottom friction. Relative to the processes listed above, the importance of short waves in storm surges was investigated more recently. Thus, Mastenbroek et al. (1993) showed that including a wave-dependant drag coefficient in the calculation of wind stress improved storm surge prediction significantly. This conclusion was then confirmed by numerous authors (Brown and Wolf, 2009; Nicolle et al., 2009; Sheng et al., 2010). In nearshore zones, the inclusion of wave radiation stress gradients allowed for a proper representation of the wave-induced setup, which can represent several tens of centimeters in the total surge (Nicolle et al., 2009; Wolf, 2009; Bertin et al., 2009b; Dietrich et al., 2010; Brown et al.,

2011). In the recent years, the inclusion of recent theories for the representation of wave-current interactions in 3D (e.g. Mellor, 2008; Ardhuin et al., 2008) suggested that 3D wave-induced circulations could impact on the total surge in nearshore zones (Xie et al., 2008; Sheng et al., 2010; Bruneau et al., 2011).

This study aims to provide firstly a detailed hindcast of the storm surge associated with Xynthia, a mid latitude storm that severely hit low-lying coasts located in the central part of the Bay of Biscay on the 27–28th of February 2010. The second objective of this study is to analyse the physical processes responsible for the surge through numerical experiments. In particular, the relative contribution of atmospheric forcing and the effect of short waves are investigated to tentatively explain why the storm surge magnitude was exceptional while the storm was not. Finally, particular attention is paid to the analysis of the development of periodic oscillations after landfall over the continental shelf.

2. The study area

2.1. Geomorphic setting

The Bay of Biscay is located in the North-East Atlantic Ocean and is bounded to the East by the western coast of France and to the South by the Northern coast of Spain (Fig. 1). The abyssal plain located in the middle has maximum depths exceeding 5000 m. The continental shelf exhibits a contrasting morphology, with a very narrow continental shelf (10–40 km wide) along the Spanish coast and a wider continental shelf along the French border, which width increases from less than 50 km to the South to more than 200 km in front of the English Channel. From South to North, the central part of the French border is interrupted by six major embayments and estuaries: the Arcachon Lagoon, the Gironde Estuary, the Pertuis d'Antioche and the Pertuis Breton (Pertuis Charentais), the Bourgneuf Lagoon and the Loire Estuary. The Pertuis d'Antioche and the Pertuis Breton are backed by extensive coastal plains, which result from intense land reclamation that occurred until the 19th century (Bertin et al., 2005). A significant part of these low-lying plains is located below high-tide level and their shorelines consist of both natural barriers and sea walls.

2.2. Hydrodynamic setting

Tides in the Bay of Biscay are semi-diurnal, with small diurnal asymmetries. Along the French shelf break, the deep-water Kelvin wave induces a M2 wave with amplitude of the order of 1.3 m (Le Cann, 1990). Throughout its propagation over the continental shelf, the M2 grows by about 10–40% and its amplitude locally reaches 1.80 m in the Pertuis Breton (Fig. 1B). Diurnal waves K1 and O1 have amplitudes of the order of 0.07 m and display little spatial variations. In contrast, quarter diurnal waves M4, MS4 and MN4 experience a huge amplification throughout their propagation over the central part of the continental shelf. Thus, offshore of the Pertuis Charentais, the amplitudes of M4, MS4 and MN4 increase from 0.027 m, 0.006 m and 0.013 m near the shelf break to 0.18 m, 0.07 m and 0.09 m by 20 m water depth, respectively. Applying the analytical model of Clarke and Battisti (1981), Le Cann, showed that for the quarter-diurnal band, the shelf was close to resonance in its central part, thereby explaining this one order of magnitude amplification. The resulting spring tidal range at the coast exceeds 6 m in the Pertuis Breton and the Pertuis d'Antioche and reaches 4.5 m to the South and 5.5 m to the North, which induces tidal currents exceeding 2 m/s in the estuaries and tidal inlets (Bertin et al., 2005).

The Bay of Biscay is fully exposed to gravity waves generated in the North Atlantic Ocean. Butel et al. (2002) and Dupuis et al.

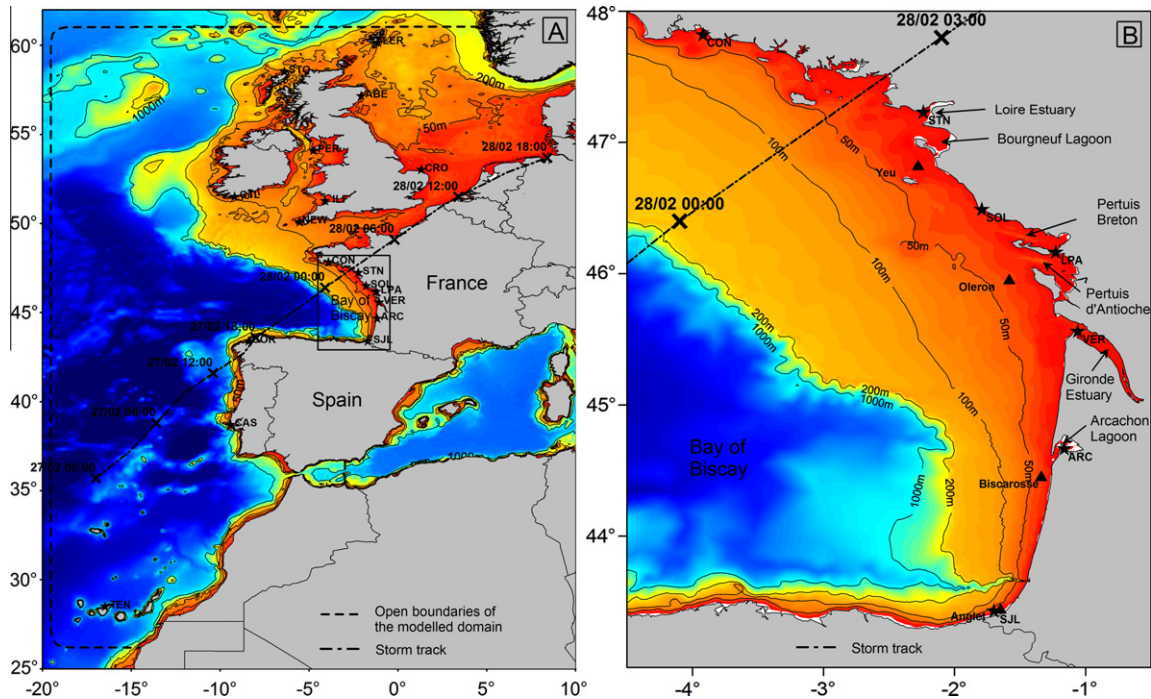


Fig. 1. A-Bathymetric map of the North-East Atlantic Ocean showing the boundary of the modeled domain, the tidal stations (stars) used for model validation and the storm track of Xynthia. B-Same as A- focused on the Bay of Biscay and locations of the wave riders (triangles). For the tidal stations, the following abbreviations were used: TEN for Tenerife (Spain), CAS for Cascais (Portugal), COR for A Coruña (Spain), SJL for Saint Jean de Luz (France), ARC for Arcachon (France), VER for Le Verdon (France), LPA for La Pallice (France), SOL for Sables D'Olonne (France), STN for Saint Nazaire (France), CON for Concarneau (France), CTL for Castletownshend (Ireland), NEW for Newlin (UK), ABE for Aberdeen (UK), ILF for Ilfracombe (UK), PER for Port-Erin (UK), CRO for Cromer (UK), STO for Stornoway (UK) and LER for Lerwick (UK).

(2006) provide a non-directional description of the wave climate in the Bay of Biscay based on the wave riders of Biscarosse (26 m water depth, Fig. 1B, data analyzed from 1980 to 2000), Yeu (33 m water depth, Fig. 1B, data analyzed from 1998 to 2000) and Biscay (4500 m water depth, 5.00°W–45.00°N, data analyzed from 1998 to 2001). The annual-mean significant wave heights H_s are 1.36 m at Biscarosse, 1.81 m at Yeu and 2.64 m at Biscay. The maximum H_s recorded over the analyzed periods are 9.70 m, 8.88 m and 13.9 m for Biscarosse, Yeu and Biscay, respectively. The annual-mean mean wave periods T_m range from 6 to 7 s at the three considered wave records, while peak wave periods T_p occasionally exceed 20 s. The wave climate inter-annual variability in the Bay of Biscay was investigated over the period 1953–2009 based on a numerical hindcast for the North Atlantic Ocean (Dodet et al., 2010), refined in the Bay of Biscay by Bertin and Dodet (2010). These studies showed that the winter-mean mean wave direction M_{wd} varies from N270° to the North to N300° to the South and its inter-annual variability is characterized by a standard deviation of the order of 5–7%. Winter-means of H_s and T_p display an inter-annual variability of the order of 20–30%, which was shown to be partly controlled by the North Atlantic Oscillation.

3. The Xynthia storm and the associated surge

Xynthia was a violent windstorm which crossed rapidly Western Europe between the 27th of February and the 1st of March 2010. Xynthia originated from a low-pressure zone located in the middle of the Atlantic Ocean around the latitude of the Tropic of Cancer. This depression intensified on the 27th in the morning and evolved towards a storm when reaching the coastlines of Portugal (Fig. 2), where instantaneous maximum wind speed exceeded 40 m/s to the North of the country. Xynthia crossed the North-Western part of the Iberic Peninsula at the end

of the day at 15–20 m/s and hit the French border of the Bay of Biscay in the night of the 28th of February, where sea-level pressure (SLP) reached its minimum at 969 mbar (Fig. 2). Southern to South-western winds ranging from 25 to 35 m/s (hourly mean at 10 m elevation) blew over the Southern part of the Bay of Biscay (Fig. 2) and maximum instantaneous values reached 45 m/s on Ré Island (Fig. 2). On the 28th of February, Xynthia pursued its way towards Belgium and Germany at 15–20 m/s and winds over the Bay of Biscay veered westward and weakened to 10–15 m/s. Meteorologically, Xynthia was not as exceptional as the storms Martin (27th of December 1999) and Klaus (23th January 2009), during which maximum winds exceeding 50–55 m/s were measured at the coast.

Xynthia generated a significant storm surge that reached its maximum in the central part of the Bay of Biscay. The largest storm surge value was recorded in La Pallice harbor (1.50 m), followed by the nearby stations of Les Sables d'Olonne to the North (1.25 m) and Graves to the South (1.05 m). Further North and closer to landfall, the maximum storm surge reached 1.02 m at Saint-Nazaire and only 0.66 m at Concarneau (Fig. 3). The storm surge maximum value also decreased to the South of the Bay of Biscay, and reached 0.75 m at Arcachon and 0.49 m at Saint Jean de Luz (Fig. 3). According to Fig. 3, the maximum storm surge occurred at the same time along the coastlines of the Bay of Biscay (around 2:00 h \pm 1 h on the 28th of February 2010), except to the South at Saint Jean de Luz where the surge maximum peaked 6–7 h in advance (around the 27th of February at 20h00). After landfall, the water level anomaly in the central part of the Bay of Biscay (stations 2–5, Fig. 3) displays 6-h oscillations with heights of the order of the order of 0.30 m.

The storm surges measured at La Pallice and Les Sables d'Olonne were the largest values ever recorded at these sites since 1949 and 1970, respectively. Nevertheless, the records at these two stations are very discontinuous before numeric tide gauges were installed (in 1997 and 1999, respectively) and were not available during

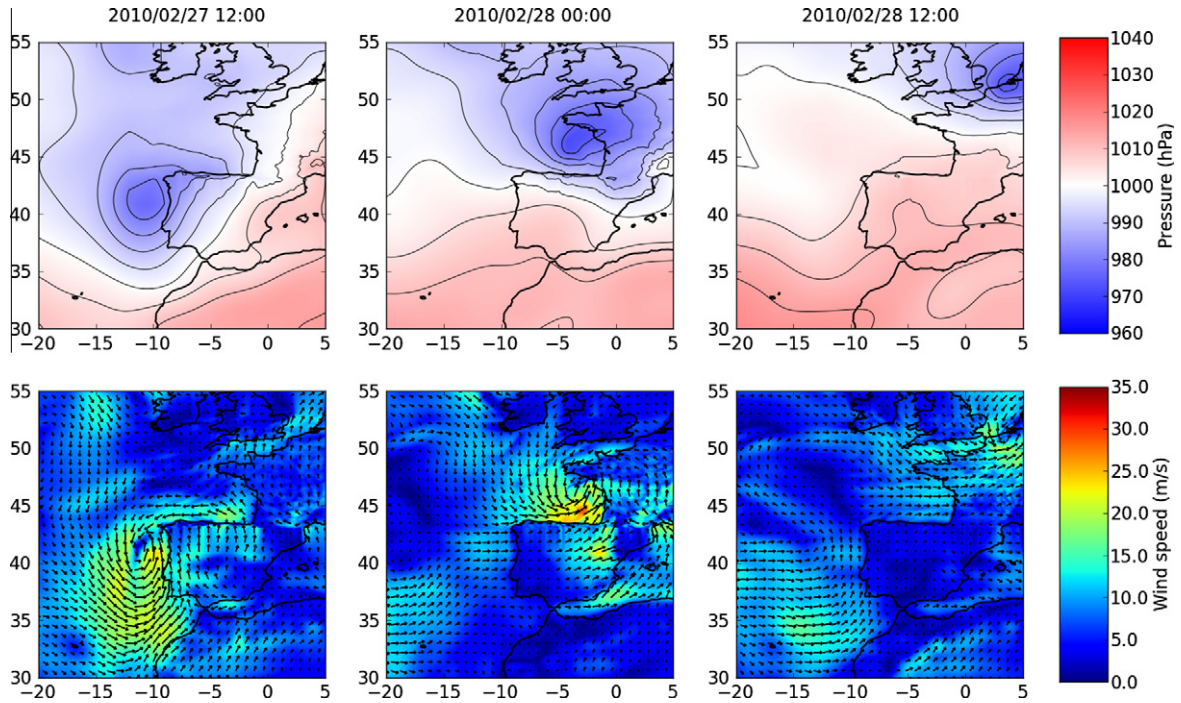


Fig. 2. Sea-level pressure and winds at 10 m during Xynthia. Data originating from the outputs of the atmospheric model Aladin (0.1°, Météo France) nested within the 0.25° GFS model (Environmental Modeling Center, 2003).

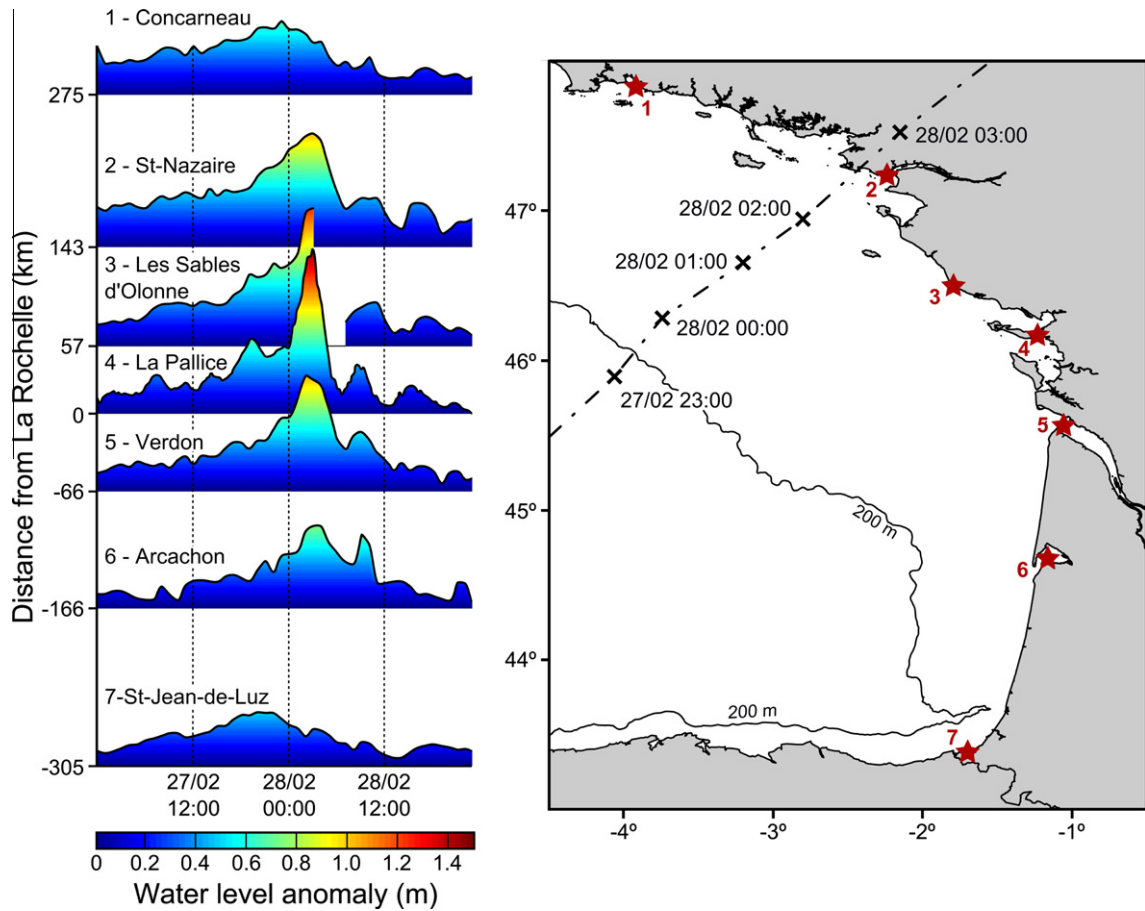


Fig. 3. Water level anomaly during Xynthia along the French coast of the Bay of Biscay, showing a maximum at La Pallice station (station 4). Stations located in the central part of the Bay of Biscay (2–5) show 6-h oscillations of the water level after landfall.

the storm Martin, which violently hit the region on the 27th December 1999 and probably caused a storm surge of the same order of magnitude as that of Xynthia (no data available). The storm surge recorded at Verdon corresponds to the second largest since 1989, but was largely exceeded during the storm Martin (1.55 m). At other stations, the maximum storm surge value reached during Xynthia is less exceptional and has a return period of 1–5 years.

Although the values for water level anomaly reached in the central part of the Bay of Biscay were exceptional (return period of the order of 20 years based on Regional Frequency Analyses by Bernardara et al. (2011) and Bardet et al. (2011), the more exceptional fact is that the maximum surge occurred at the time of spring-tide high water. The corresponding total water level reached 8.01 m above marine chart datum in La Pallice, which value was shown to have a return period larger than 100 years (Simon, 2008). Many natural barrier and sea-walls were submerged and/or breached, causing the flooding of very large areas, some of which were inhabited. 47 people tragically died and material damages were estimated at 1.5 billion Euros.

4. Data and methods

4.1. The storm surge numerical model

In this study, we built a storm surge modeling system that couples externally (i.e. variables are exchanged between the two models through binary files) the state-of-the-art circulation models SELFE (Zhang and Baptista, 2008) and WaveWatchIII (Tolman, 2009).

4.1.1. The wave model

Gravity waves generation and propagation were simulated with the WaveWatchIII model (WWIII, version 3.14; Tolman, 2009), which is a 3rd generation model solving the wave energy balance equation (Hasselmann, 1974) by means of finite differences on regular structured grids. In the present study, the effects of currents on wave propagation were neglected, thus the resolved equation in spherical coordinates reads:

$$\begin{aligned} \frac{\partial N}{\partial t} + \frac{\partial}{\partial \lambda} \left(\frac{c_g \sin \theta}{R \cos \phi} N \right) + \frac{1}{\cos \phi} \frac{\partial}{\partial \phi} \left(\frac{c_g \cos^2 \theta}{R} N \right) \\ - \frac{\partial}{\partial k} \left(\frac{\partial \sigma}{\partial d} \frac{\partial d}{\partial s} N \right) - \frac{\partial}{\partial \theta} \left(\frac{N}{k} \frac{\partial \sigma}{\partial d} \frac{\partial d}{\partial m} + \frac{c_g \tan \phi \cos \theta}{R} N \right) \\ = \frac{S_{tot}}{\sigma} \end{aligned} \quad (1)$$

where t is time, λ and ϕ are the longitude and latitude respectively, σ is the relative wave frequency, k is the wave number and θ is the wave direction. N is the wave action density, c_g is the wave group velocity, d is the mean depth, R is the radius of the Earth and s and m correspond to the collinear and perpendicular coordinates to the wave propagation direction, respectively. The source terms S_{tot} represents wave growth by wind and wave decay due to white-capping, wave breaking and bottom friction. The parameterizations used for wave growth and whitecapping correspond to that of “Test 350” described in Ardhuin et al. (2010). A recent inter-comparison of the results obtained by the main prediction centers around the world revealed that the last version of WWIII, which includes the recent developments of Ardhuin et al. (2010), was the most accurate (Bidlot, 2008).

WWIII also provides the friction velocity u_{*s} , required to compute the surface stresses of the hydrodynamic model. This friction velocity is calculated according to the formulation of Tolman and Chalikov (1996) and Tolman (2009). Assuming that the mean wind profile has a logarithmic shape (except in a thin surface near the

surface ocean), the velocity at a distance z above the water surface can be written:

$$u_z = \frac{u_*}{\kappa} \ln \left(\frac{z}{z_0} \right) \quad (2)$$

where $\kappa = 0.4$ is the von Kármán constant and z_0 is the effective roughness parameter expressed by:

$$z_0 = \chi \sqrt{\alpha} \frac{u_*^2}{g} \quad (3)$$

with χ a constant set to 0.2 and α the Phillips conventional non-dimensional energy level at high frequencies. Combining Eqs. (2) and (3), the drag coefficient C_z at the z level becomes (Chalikov, 1995):

$$C_z = \left(\frac{u_*}{u_z} \right)^2 = \kappa^2 [R - \ln(C_z)]^{-2} \quad (4)$$

$$R = \ln \left(\frac{zg}{\chi \sqrt{\alpha} u_z^2} \right) \quad (5)$$

R is a non-dimensional parameter (Chalikov and Belevich, 1993). Finally, the parameter α is estimated parametrically according to Janssen (1989):

$$\alpha = 0.57 \left(\frac{u_*}{c_p} \right)^{3/2} \quad (6)$$

where c_p is the wave phase velocity and the ratio u_*/c_p is the inverse of the wave age W_a . Eq. (4) is then accurately approximated (Tolman, 2009) as:

$$C_z = 10^{-3} \left(0.021 + \frac{10.4}{R^{1.23} + 1.85} \right) \quad (7)$$

An important consequence of this parameterization is that C_z is an hyperbolic decreasing function of the W_a . As the last equations depend on the drag coefficient, an iterative method is used to solve the problem at the initialization. Assuming the friction velocity evolves slowly, the iterative method is not necessary during the time stepping.

A 0.1° regular grid was emplaced over the whole domain (Fig. 1A), which resulted in 122,094 nodes (323 by 378). This resolution was sufficient to reproduce adequately wave shoaling, refraction and dissipation by bottom friction on the shelf, but does not allow for a proper representation of surf-zones. The spectral space was discretized according to 24 equally spaced directions and 25 frequencies ranging from 0.041 Hz and 0.41 Hz with a logarithmic increment. The maximum global time step and the CFL propagation time step were set to 300 s. The model was forced over the whole domain by 3-hourly wind fields having a 0.25° resolution and originating from the GFS model (Environmental Modeling Center, 2003) and linearly interpolated over a 0.1° grid with a hourly time step. Hourly wind fields with a 0.1° resolution and originating from the Aladin – Meteo France model (Bénard, 2004) were nested over the whole Bay of Biscay and the English Channel. The model was forced along its open boundaries by wave spectra originating from the regional wave model of Dodet et al. (2010), forced by wind fields originating from the ERA-Interim reanalysis (Simmons et al., 2006).

4.1.2. The circulation model

The numerical model SELFE (Zhang and Baptista, 2008) solves the shallow water equations in 3D and was designed to simulate circulation and tracer evolutions for a large range of spatial scales and types of environments, spanning from very shallow lagoons and estuaries (Rodrigues et al., 2011) to large estuaries (Zhang and Baptista, 2008; Liu et al., 2011) and to continental

shelves and open ocean (Fortunato et al., 2011). The continuity equation is solved using a finite volume method while the momentum equations are solved using a Galerkin finite element method, based on an unstructured grid. The Lagrangian treatment of advective terms and a semi-implicit method insures numerical stability, even using large hydrodynamic time steps. SELFE uses a natural treatment of wetting and drying, which makes it suitable for inundation studies. The code is parallelized and uses PARMETIS domain-decomposition (<http://glaros.dtc.umn.edu/gkhome/metis/parmetis/overview>) to distribute the global mesh over several computational cores with the MPI (Message Passing Interface) protocol. In the present application, SELFE was used in 2-dimensional horizontal (2DH) barotropic mode. Considering the selected physical processes, and denoting by η the surface elevation and by \vec{u} the horizontal velocity, the corresponding equations read:

$$\frac{\partial \eta}{\partial t} + \vec{\nabla} \cdot \int_{-h}^{\eta} \vec{u} dz = 0 \quad (8)$$

$$\frac{D\vec{u}}{Dt} = -f\vec{k} \times \vec{u} + \alpha g \vec{\nabla} \psi - \frac{\vec{\nabla} P_A}{\rho} - g \vec{\nabla} \eta + \frac{\vec{\tau}_S - \vec{\tau}_B}{\rho(\eta + h)} \quad (9)$$

where h the bathymetry, ρ is water density, f is the Coriolis factor, P_A is the sea-level atmospheric pressure, and α and ψ are the effective earth-elasticity factor and the earth tidal potential, respectively. Finally, $\vec{\tau}_B$ is the bottom stress computed using a quadratic friction law and $\vec{\tau}_S$ is the wind stress defined as:

$$\vec{\tau}_S = (\rho_a u_*^2) \quad (10)$$

where ρ_a is the air density.

At such large scale applications, spherical coordinates are preferably required because large errors occur with map projections. The strategy developed in SELFE and initially proposed by Comblen et al. (2009) consists in using a series of local frames at the different locations of the unstructured meshes, which permit to use the normal Cartesian system of coordinates with only simple coordinate transformations (Zhang et al., 2011).

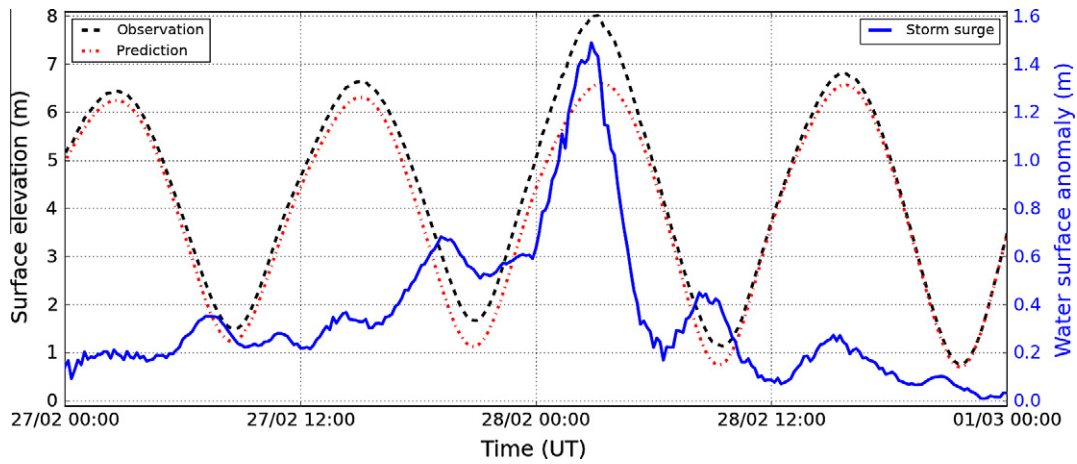


Fig. 4. Observed vs predicted water levels at La Pallice, showing a 1.50 m storm surge peak in phase with spring high tide.

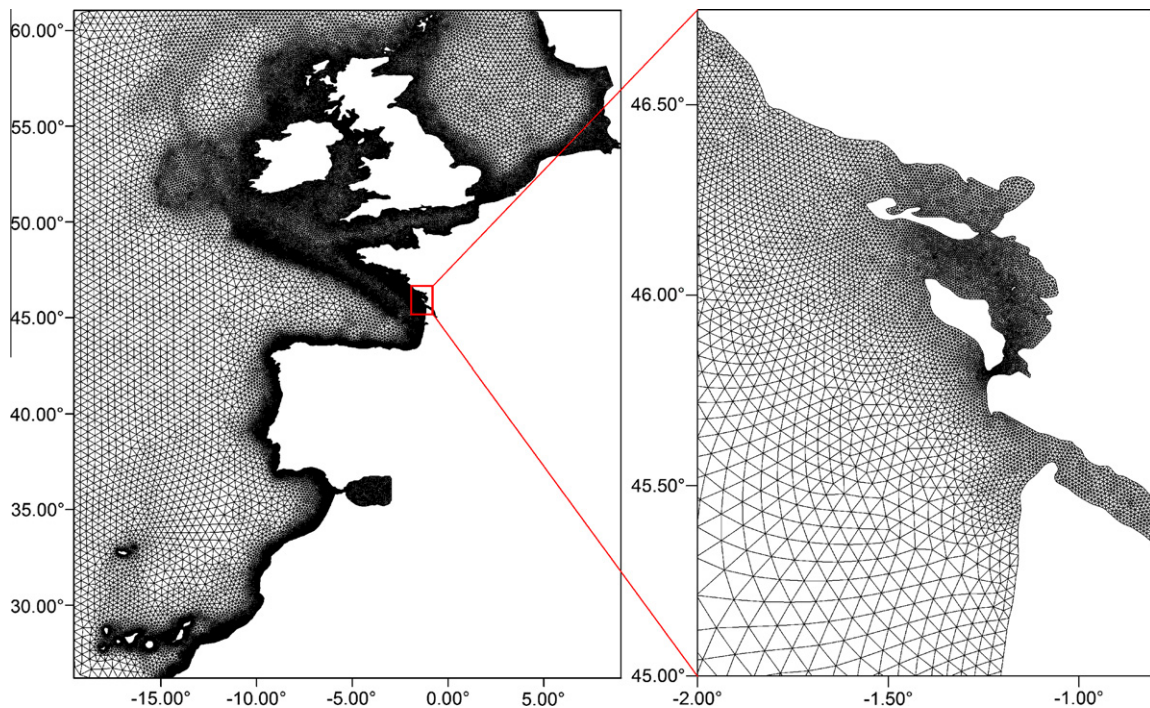


Fig. 5. The unstructured computational grid used to discretize the North-East Atlantic Ocean.

The geographical space is discretized by means of a 52,000 node unstructured grid (110,000 triangular elements) and extending from the Canary Islands to the South (20°N) to the North Sea to the North (61°N) and to –20° the West and to the Scandinavian Peninsula to the East (10° W) (Fig. 5). Such a large geographical extension was selected after several sensitivity tests on smaller grids, which did not permit to reproduce adequately the inverse barometric effect. The resolution of this grid ranges from 0.3° over abyssal plains to 0.02° on the shelf breaks and reaches 0.0025° around La Rochelle. The corresponding 250 m resolution does not allow for an adequate representation of dykes and natural barriers, which are typically 10–50 m wide. Thus, the areas flooded during Xynthia are not included in the present grid. The post-processing routine developed by Fortunato et al. (2011) was applied to the grid in order to improve its orthogonality. A 300 s hydrodynamic time-step was selected after several sensitivity tests in the range 60–600 s.

The model was forced by the astronomic tidal potential over the whole domain for the tidal constituents MM, MF, O1, K1, P1, Q1, M2, S2, N2 and K2. The model is also forced along its open boundaries by the 18 main tidal constituents of the region (O1, K1, P1, Q1, M2, S2, N2, K2, 2N2, L2, MU2, NU2, M4, MS4, MN4 and M6) obtained by linear interpolation of the regional tidal model of Pairaud et al. (2008). For storm surge applications, the model was forced over the whole domain by sea-level pressure fields originating from the same GFS-ALADIN combination and using the same procedure as for the wind-wave model. The coupling with WaveWatchIII was realized through the wind friction velocity U_w , linearly interpolated over the unstructured grid with a 300 s update. For the numerical experiments of Section 6.2, the model was also forced by wind fields originating from the GFS-ALADIN combination.

4.2. Field data

Sea-surface elevation data were collected at 17 stations spread over the whole modeled domain (Fig. 1) and available at the SONEI (www.sonei.org) and BODC (www.bodc.ac.uk/) databases. In order to calibrate and validate the tidal model, a common procedure was applied to the data from each station over the 2010 time-series. A harmonic analysis followed by a harmonic synthesis using the 59 main tidal constituents was performed using R_T_Tide (Leffler

and Jay, 2009) to remove the non-astronomic component of the elevation and allow for a consistent comparison with model results. For the seven stations located in the Bay of Biscay, the residual between the observed and synthesized elevation was computed to characterize the storm surge alongshore variability during Xynthia.

Wave conditions in the Bay of Biscay during Xynthia were characterized by means of three Datawell wave riders, deployed by CETMEF (French division for Fluvial and Maritime technical studies) at Anglet (25 m water depth), Yeux Island (32 m water depth) and by SHOM (French Naval Oceanographic Service) to the west of Oléron Island (35 m water depth).

5. Model validation

5.1. Tidal predictions

Our new regional tidal model was calibrated varying the friction coefficient C_d in the quadratic friction parameterization and best agreements were obtained using the uniform value of $C_d = 0.0025$ over the whole domain. SELFE was run over the whole year 2010 in order to meet the Rayleigh criterion and separate properly K2 from S2 (299 days at least). The model was then validated by comparing predicted against observed tidal amplitudes and phases for the 18 main tidal constituents imposed along its open boundaries. This comparison is presented in Table 1 for the main diurnal (O1), semi-diurnal (M2) and over-tide (M4) constituents at 17 stations spread over the modeled domain (Fig. 1, stars). For the stations located along the Atlantic Ocean (Tenerife, Cascais, A Coruña, St Jean de Luz, Verdon, La Pallice, Les Sables d'Olonne, Saint Nazaire and Concarneau; Fig. 1), amplitudes and phases are very well reproduced, with errors included in the ranges 0.00–0.03 m and 0–15°, respectively (Table 1). For stations located along the Channel Island, the North Sea and the Irish Sea (Newlin, Ilfracombe, Port-Erin, Cromer, Aberdeen, Lerwick, Stornoway and CastleTownsend; Fig. 1), discrepancies between model and data are slightly larger, being included in the ranges 0.00–0.15 m and 0–20°, for amplitudes and phases respectively (Table 1).

The model was then validated for the total elevations, which namely allows quantifying the impact of forcing the model with 20 constituents only. Thus, for the 17 selected stations, Root Mean Square Discrepancies (RMSD) were computed for elevation time-series synthesized from 59 constituents (harmonic analysis from

Table 1
Predicted against observed tidal amplitudes and phases for the main diurnal (O1), semi-diurnal (M2) and quart-diurnal (M4) constituents at 17 stations spread over the modeled domain. Root Mean Square Error on the total elevation and scatter index, defined as the RMSE normalized by the mean tidal range for each site.

Station name	O1				M2				M4				Total elevation	
	Amplitude (m)		Phase (°)		Amplitude (m)		Phase (°)		Amplitude (m)		Phase (°)		RMSD (m)	SI(–)
	Obs.	Model	Obs.	Model	Obs.	Model	Obs.	Model	Obs.	Model	Obs.	Model		
Tenerife (Canary)	0.06	0.05	299	304	0.70	0.69	28	29	0.01	0.01	105	133	0.03	0.02
Cascais (Portugal)	0.06	0.06	325	324	0.98	0.98	64	62	0.01	0.02	187	181	0.03	0.01
A Coruna (Spain)	0.08	0.07	335	331	1.15	1.18	88	85	0.01	0.01	288	297	0.08	0.03
St. Jean de Luz (France)	0.07	0.07	331	332	1.32	1.34	91	91	0.03	0.03	324	333	0.06	0.02
Verdon (France)	0.08	0.08	342	340	1.56	1.60	108	106	0.08	0.10	353	2	0.09	0.03
La Pallice (France)	0.08	0.08	336	337	1.73	1.71	96	96	0.25	0.26	5	9	0.08	0.02
Sables d'Olonne (France)	0.08	0.08	349	338	1.54	1.55	94	95	0.15	0.16	11	3	0.06	0.02
St. Nazaire (France)	0.08	0.08	340	338	1.71	1.68	107	97	0.18	0.18	50	26	0.08	0.02
Concarneau (France)	0.07	0.07	340	328	1.45	1.47	94	95	0.06	0.07	37	31	0.07	0.02
Newlin (UK)	0.06	0.06	339	1.03	1.73	1.63	102	123	0.11	0.07	103	121	0.09	0.04
Ilfracombe (UK)	0.07	0.07	1	5	3.00	2.91	160	164	0.11	0.10	346	322	0.15	0.04
Port-Erin (UK)	0.11	0.10	52	56	1.82	1.76	320	316	0.01	0.02	78	113	0.10	0.08
Cromer (UK)	0.17	0.16	143	157	1.51	1.55	202	186	0.08	0.09	324	274	0.11	0.03
Aberdeen (UK)	0.13	0.13	61	67	1.29	1.30	23	24	0.03	0.03	264	323	0.08	0.03
Lerwick (UK)	0.09	0.07	34	46	0.56	0.64	311	311	0.01	0.03	275	314	0.10	0.08
Stornoway (UK)	0.11	0.09	354	353	1.33	1.16	197	195	0.06	0.01	218	213	0.17	0.06
Castle townsend (Ireland)	0.02	0.02	293	309	1.09	1.13	129	137	0.03	0.01	276	196	0.09	0.04

2010 elevation data). In order to compare consistently model skill from one station to another, a Scatter Index (SI) was defined as the ratio between the RMSD and the mean tidal range at each station. In accordance with the validation performed on constituent amplitudes and phases, the model performs best at the stations located along the Atlantic Ocean, with RMSD and SI included in the ranges 0.03–0.09 m and 1–3%, respectively. The model also performs slightly worse in the English Channel, the North Sea and the Irish Sea, with RMSD and SI included in the ranges 0.09–0.17 m and 3–8%, respectively. Among the various hypotheses to explain the relatively weaker predictive skills of the model in the northern part of the modeled domain, it can be argued that it originates from the resolutions of the unstructured grid as well as of the bathymetric data, which are too coarse to represent adequately the complex coastal morphology around UK and Ireland. Another limitation could be related to the use of a uniform bottom drag coefficient, while most of the stations are bordered by shallow and extensive continental shelves where strong tidal currents occur. Nevertheless, these errors are acceptable, particularly in the scope of the present study focused on the Bay of Biscay, where model predictions are very good.

5.2. Wave predictions

WWIII predictions were compared against data sampled offshore the Oléron Island, which corresponds to the region where the largest storm surge occurred (Figs. 3 and 4). Fig. 6 shows that the model is able to reproduce quite satisfactory the temporal evolution of mean wave parameters around Xynthia, with RMSD of 0.45 m, 13° and 2 s for significant wave height (H_s), peak direction (P_{dir}) and peak period (T_p), respectively. Once normalized by the data, the RMSD result in scatter indexes of 16% and 15% for H_s and T_p , respectively. The model captures well the different peaks of H_s , with only a slight underestimation (bias of -0.09 m). During

Xynthia, the wave peak direction shifts rapidly from W (N260°) to S (N160°) while T_p drops to 6 s, but these behaviors are also well captured by the model. The model globally performs very well during Xynthia, although this storm was characterized by very steep ($H_s = 7$ m vs $T_p = 7-10$ s) and young waves ($W_a = 9$). This performance is noteworthy and can be attributed to recent improvements of dissipation terms in WWIII (Ardhuin et al., 2010),

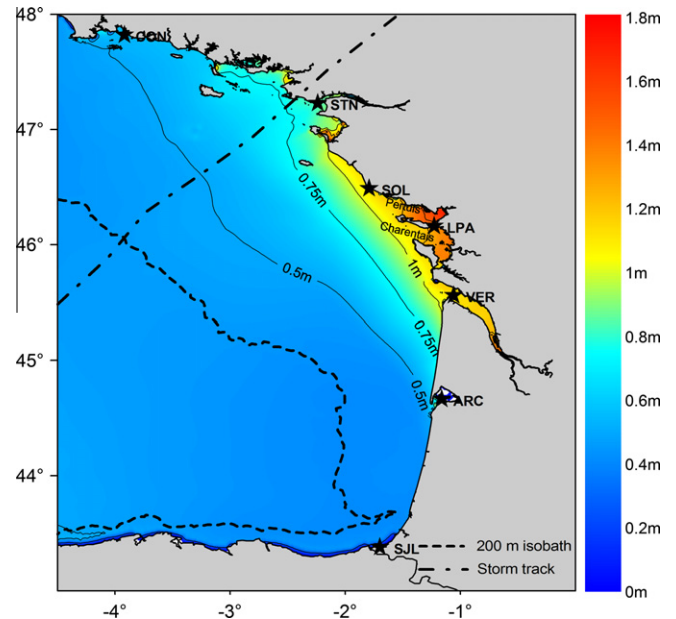


Fig. 7. Contour map of the modeled maximum storm surge in the Bay of Biscay, showing a maximum of 2.0 m in the inner part of the Pertuis Charentais. The dashed line corresponds to the 200 m isobath line and represents the continental shelf break.

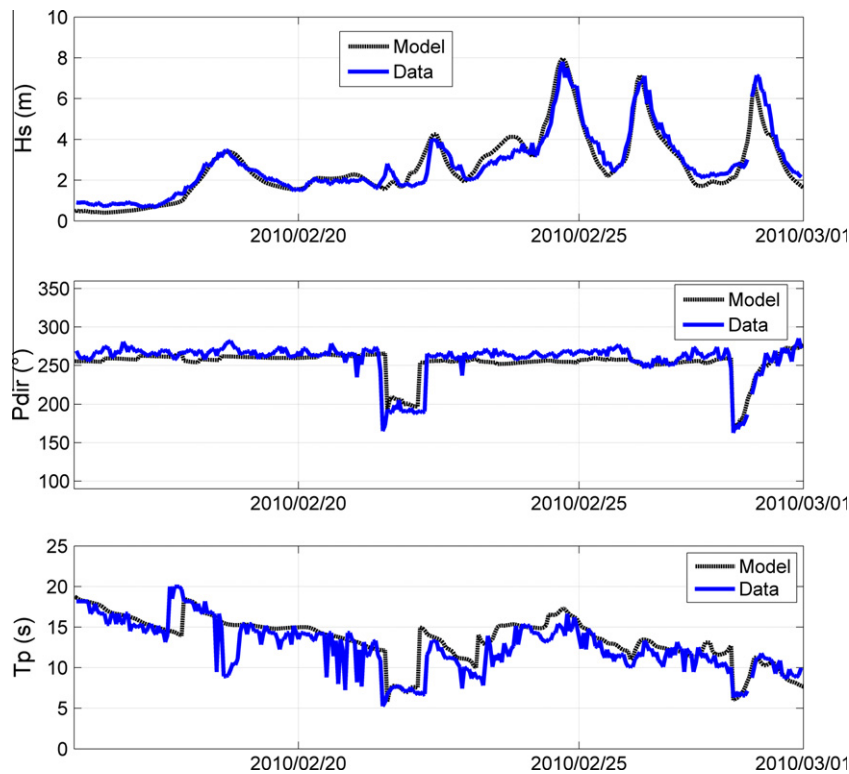


Fig. 6. Times series of wave characteristics (H_s , P_{dir} and T_p) at the Oléron buoy (dark plain triangle on Fig. 1b), near La Rochelle. Comparisons between the data (dashed black line) and model predictions (solid blue line). (For interpretation of the references to color in this figure legend, the reader is referred to the web version of this article.)

before which such young and steep waves were often strongly overestimated (Ardhuin et al., 2009).

5.3. Storm surge predictions

The maximum values of the predicted storm surge in the Bay of Biscay are shown on Fig. 7. This figure shows firstly that the storm surge is less than 0.5 m outside the continental shelf and progressively increases with shallower depths. Storm surge exceeds 1.0 m in the central part of the Bay of Biscay and reaches its maximum in the inner part of the Pertuis Charentais (around 1.75 m).

The predictions of the water surface anomalies were compared against observations at six different locations in the Bay of Biscay over a two day windows centered on Xynthia (Fig. 8). Both in terms of peak magnitude and phase, the model succeeds to reproduce quite satisfactorily the surge induced by Xynthia in the Bay of Biscay. Considering the three stations where the surge was the largest (Les Sables d'Olonne, La Pallice and Le Verdon), the peak deviations and the phase lags between the model and the data are of around -6% , -8% and 3% and -30 min, 40 min and 30 min, respectively. The RMSD and bias were calculated at the stations over this two-day period (Table 2) and were included in the ranges 0.12–

0.17 m and -0.13 to -0.01 m, respectively. In more details, a 0.10–0.20 negative bias was obtained at every station about 24 h before landfall. The model also succeeded to reproduce the development of 6-h oscillations that occurred in the central part of the Bay of Biscay after landfall (St Nazaire, Les Sables d'Olonne, La Pallice and Verdon, Fig. 8).

6. The physical processes controlling the storm surge during Xynthia

6.1. The impact of atmospheric forcings

In order to evaluate the respective contributions of wind and atmospheric sea-level pressure gradients (SLP) in the whole storm surge, synthetic numerical simulations were performed, considering SLP only (Fig. 9 – curve a), wind only (Fig. 9 – curve b), the algebraic sum of both contributions (Fig. 9 – curve c) and these results were compared against the baseline simulation that includes winds and SLP (Fig. 9 – curve d).

These numerical experiments show firstly that the sum of the contributions of SLP and wind effects closely matches the baseline simulation, which suggests the insignificance of non-linear

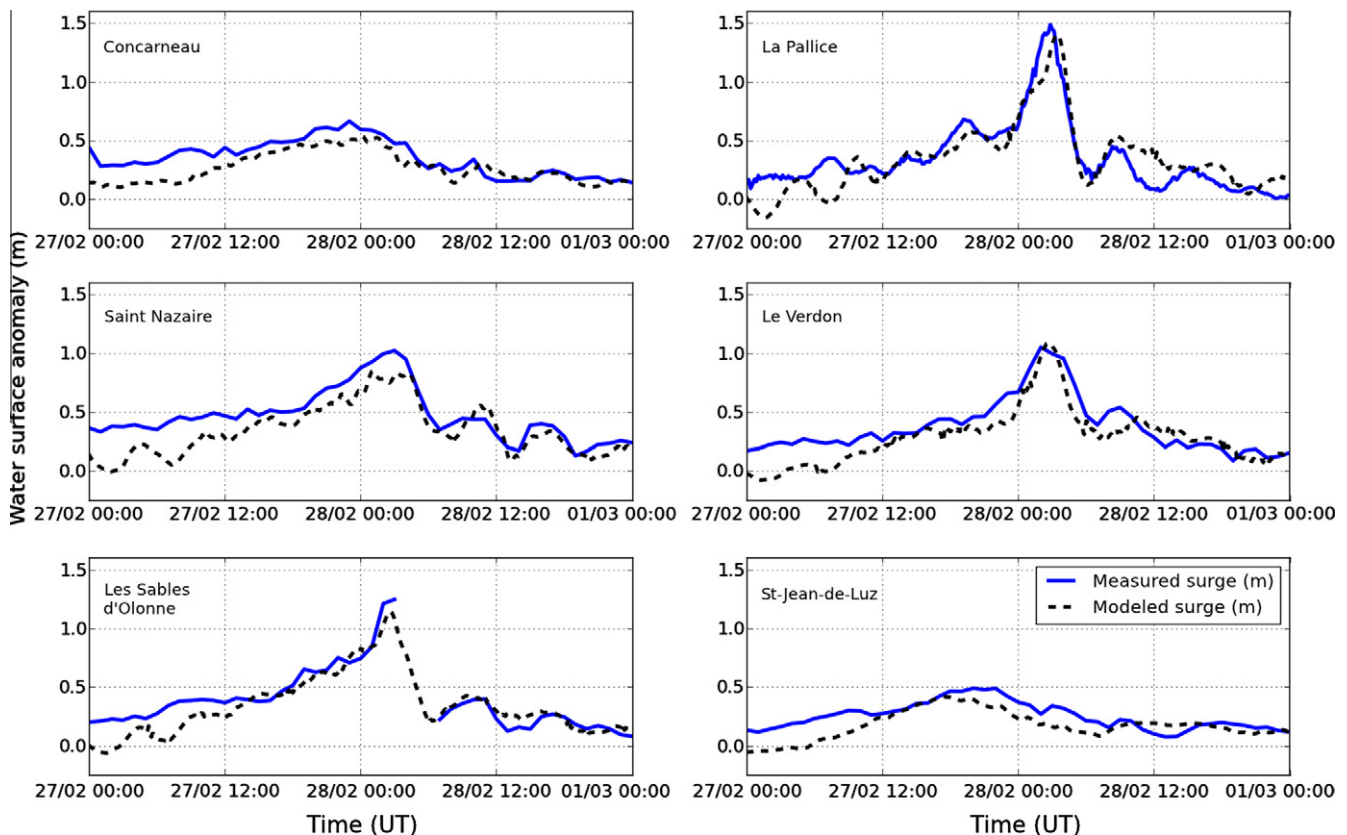


Fig. 8. Predicted (solid blue line) against observed (dashed black line) water level anomaly at Concarneau, St Nazaire, Les Sables d'Olonne, La Pallice, Le Verdon and St Jean de Luz stations, showing a good agreement between model and data. (For interpretation of the references to color in this figure legend, the reader is referred to the web version of this article.)

Table 2

Statistical results of modeled/observed surge comparisons for a set of seven stations (stars in Fig. 3b) located in the Bay of Biscay: station name, Root Mean Square Discrepancies (RMSD) and Bias.

Stations	Concarneau	Saint-Nazaire	Les Sables d'Olonne	La Pallice	Verdon	Saint-Jean-de-Luz
RMSD (m)	0.12	0.17	0.12	0.16	0.15	0.12
Bias (m)	-0.086	-0.129	-0.054	-0.014	-0.092	-0.079

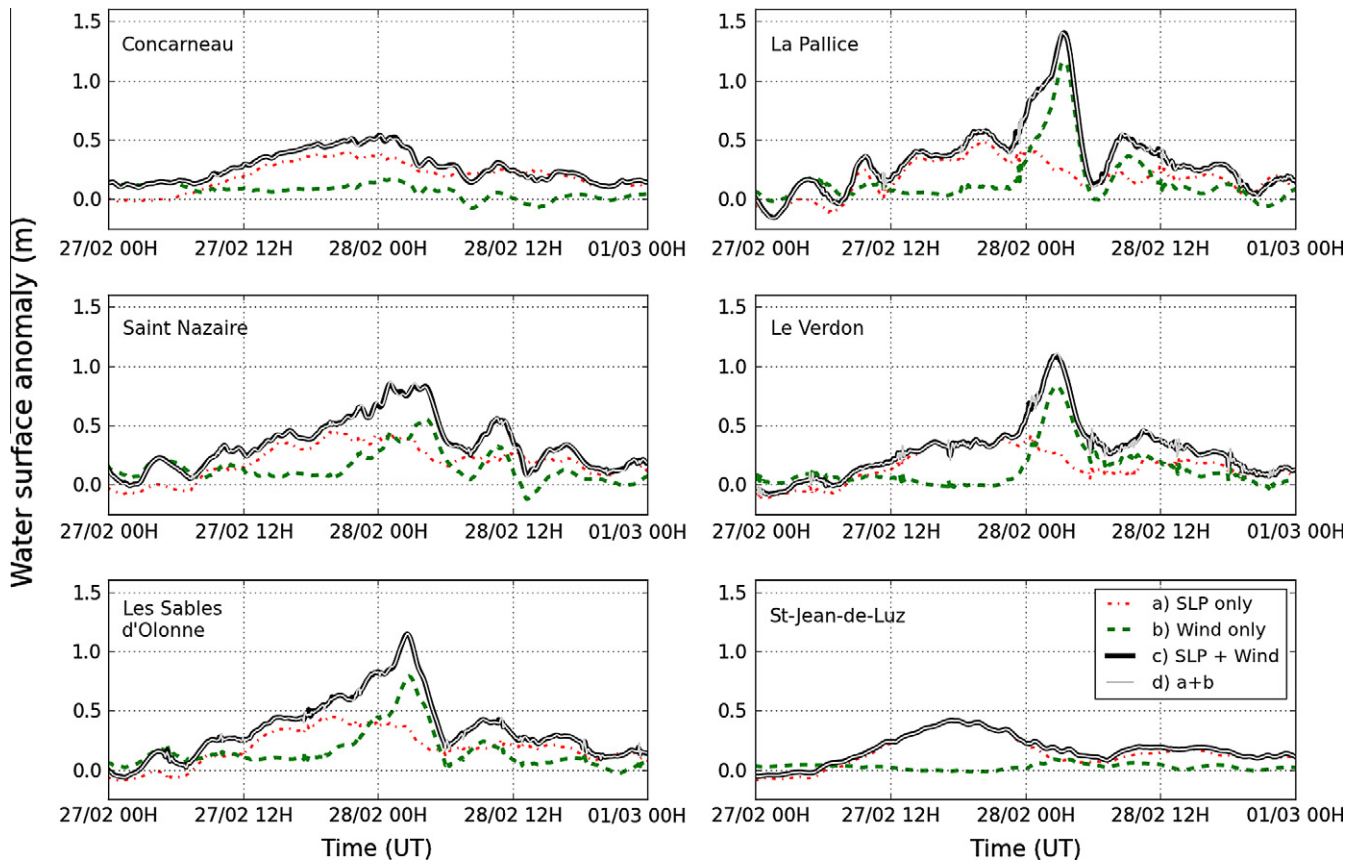


Fig. 9. Time series of water level anomalies computed considering (a) SLP only, (b) wind only, (c) SLP and wind and sum of (a) and (b).

interactions between SLP and wind. At Concarneau and St Jean de Luz, SLP drives 70–100% of the total storm surge. The weak contribution of wind at Concarneau can be explained by its offshore orientation during a large part of the storm (Fig. 2), while at Saint Jean de Luz, it can be related to the very narrow continental shelf (Fig. 1B). At Saint-Nazaire (Fig. 1), which is the station closest to landfall and thus exposed to the lowest SLP, wind and SLP have roughly an equivalent contribution in the whole storm surge. In the central part of the Bay of Biscay (Sables d'Olonne, La Pallice and Verdon; Fig. 1), the wind effect is clearly dominant upon SLP and drives between 70% and 80% of the whole storm surge. These results corroborate previous studies, which showed that wind stress is the dominant factor in the generation of storm surge in shallow waters (Jelesnianski, 1966; Rego and Li, 2010).

In the northern hemisphere, the Coriolis Effect causes the main storm surge to peak to the right side of the storm track at landfall (Kennedy et al., 2011). In order to verify this hypothesis in the case of Xynthia, a synthetic simulation was performed turning off the Coriolis force into SELFE and comparing it with the baseline simulation (Fig. 10).

This test shows that turning off the Coriolis force reduces the whole storm surge by 20–30% at the four stations located in the central part of the Bay of Biscay and where the largest storm surge occurred. This behavior demonstrates that a significant part of the surge was due to a Coriolis-induced Ekman transport, related to the South to South-west oriented wind.

6.2. The impact of waves

The storm surge model ran at the earliest stage of this study utilized the quadratic parameterization of Zeng et al. (1998) to compute wind stresses and systematically underestimated the surge

peak by 20–30% in the central part of the Bay of Biscay. This simpler parameterization is compared against our baseline simulation (Fig. 11), which utilizes a wave-dependant parameterization to compute wind stress (Section 4.1.1). This comparison shows that the two approaches perform similarly except during the storm peak, where the surge with the wave-dependant parameterization for wind stress is 30% larger. Several studies (Mastenbroek et al., 1993; Zhang and Li, 1996; Moon, 2005; Brown and Wolf, 2009; Nicolle et al., 2009; Sheng et al., 2010; Brown et al., 2011) already showed that calculating the wind stress with a wave-dependant parameterization amplified the storm surge by 10–20%. In order to explain the stronger-than-normal wave dependence of the storm surge during Xynthia, the friction velocity U_* and wave age W_a are plotted on Fig. 11B. A significant drop in W_a occurred during Xynthia, which resulted in a large increase in the friction velocity U_* . Such young waves can be related to the unusual storm track associated with Xynthia, which crosses the Bay of Biscay from SW to NE, thereby resulting in a restricted fetch that produced very steep ($H_s = 7$ m vs $T_p = 7$ –10 s) and young waves.

Other wave-related processes can have a significant impact on the storm surge at the coast. Thus, several studies showed that the onshore component of wave radiation stress gradients (Longuet-Higgins and Stewart, 1964) produce a wave setup that can contribute significantly to the whole storm surge (Xie et al., 2008; Nicolle et al., 2009; Wolf, 2009; Liu and Xie, 2009; Sheng et al., 2010; Dietrich et al., 2011). The adequate representation of wind-waves in surf zones in WWIII and their radiation stress gradient in SELFE requires a spatial resolution finer than 50–100 m along the coast, which would result in a computational grid for SELFE with over a million nodes in the case of the whole Bay of Biscay. Although it was shown recently that such computations were possible using massive parallel techniques (Dietrich et al., 2010, 2011;

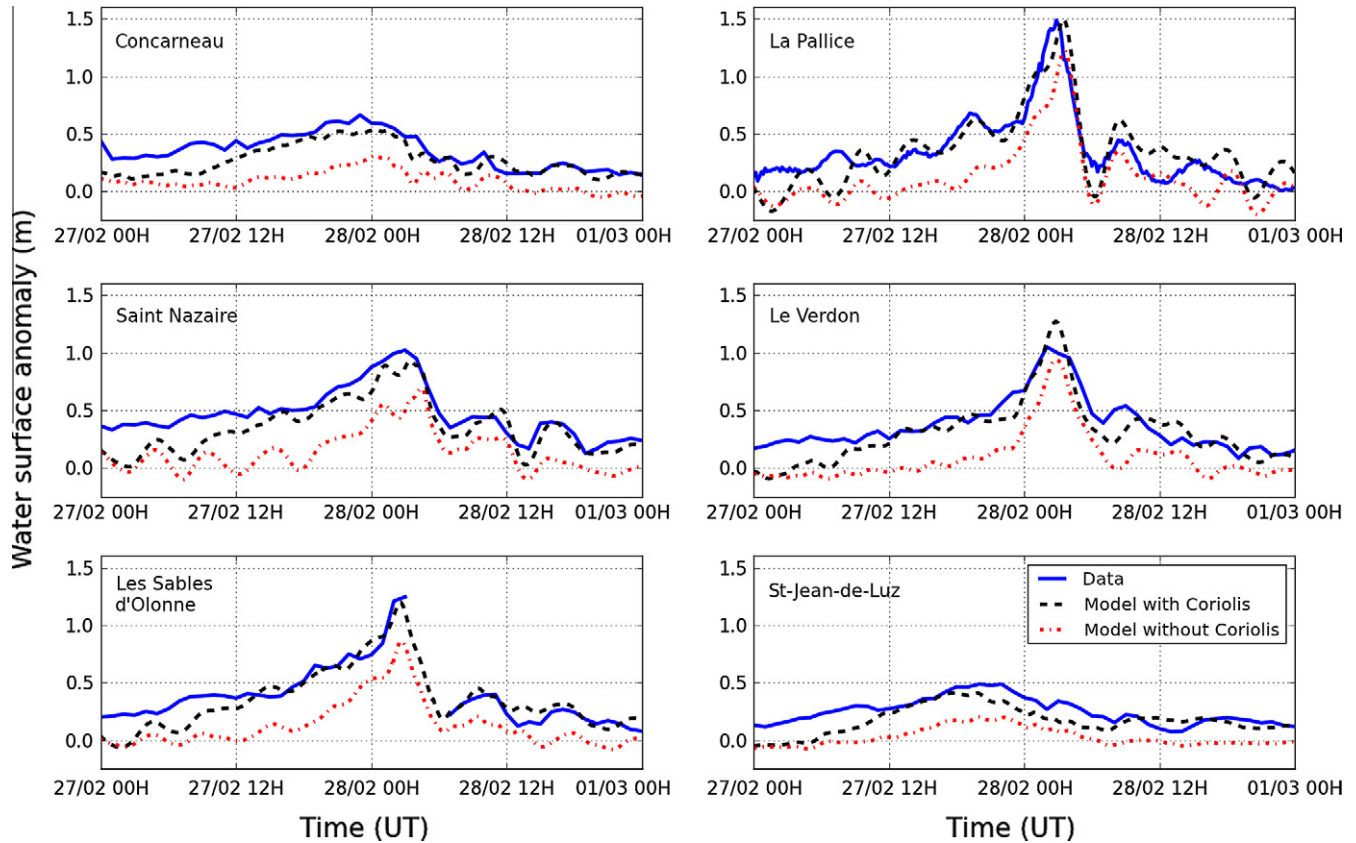


Fig. 10. Time series of measured (solid blue line) and computed water level anomalies with (dashed black line) and without Coriolis effect (dashed-dotted red line), which shows that at most stations, the wind direction and the Coriolis-induced Ekman transport are responsible for a large part of the storm surge. (For interpretation of the references to color in this figure legend, the reader is referred to the web version of this article.)

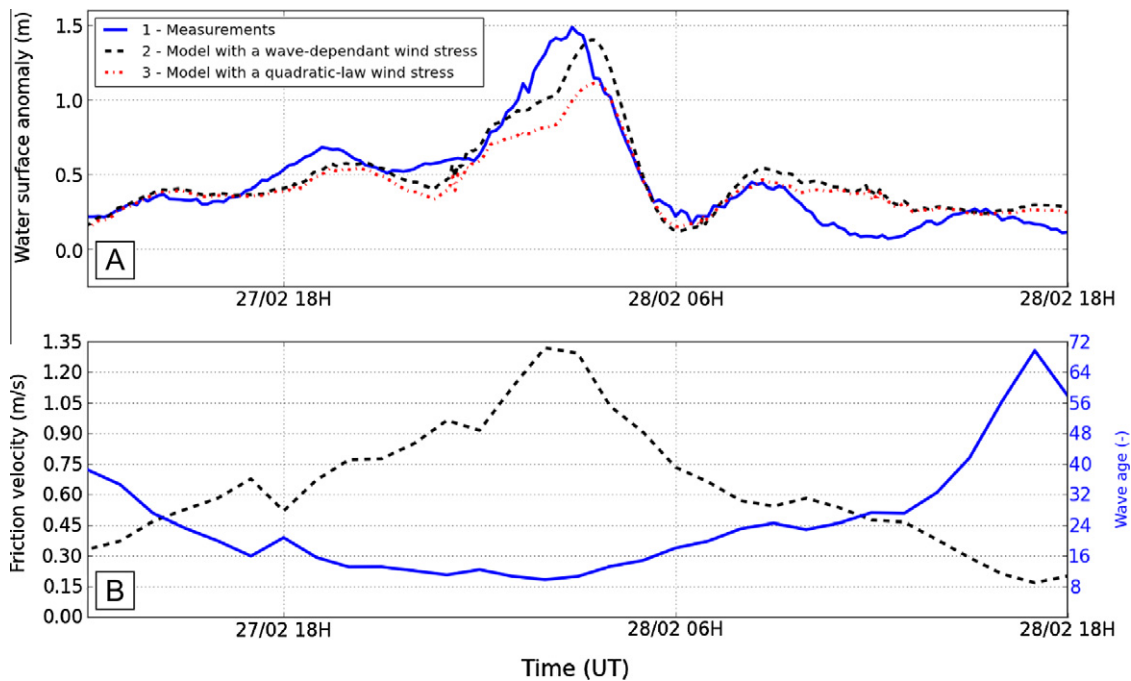


Fig. 11. (A) Time series of measured (1 – solid blue curve) and computed water level anomalies with a wave-dependant (2 – dashed black line) and a quadratic (3 – dashed dotted red line) parameterization to compute wind stress. (B) Time series of wave age W_a (solid blue line) and friction velocity U_* (dashed black line) at the Oléron wave rider, showing a drop of W_a and a peak of U_* during Xynthia. (For interpretation of the references to color in this figure legend, the reader is referred to the web version of this article.)

Bunya et al., 2010), this would fall outside the scope of the present study. Nevertheless, the application of a well-validated 2DH morphodynamic modeling system fully coupling waves and currents in the Pertuis Charentais area (Bertin et al., 2009a; Poirier et al., 2010) revealed that wave radiation stresses during Xynthia increased water levels in La Pallice by 0.05–0.08 m (not presented here). Other studies suggested that wave-induced bottom stress can slightly decrease storm surge magnitude (Xie et al., 2008; Nicolle et al., 2009; Sheng et al., 2010). In the Pertuis Charentais area, this effect was shown to be more significant in very shallow areas (Nicolle et al., 2009). Sensitivity tests on the bottom drag coefficient C_d of the circulation model confirmed that bottom stress has only a limited impact on storm surge magnitude at the stations considered in this study (not presented here). These stations are all closely connected to channels with water depths of over 20 m, which explains this weak impact of bottom stress. The impact of wave-induced bottom stress will have to be further investigated in very shallow areas and inner estuaries.

6.3. Storm surge resonance on the continental shelf

Both modeled and measured storm surges display the development of oscillations after landfall with heights ranging from 0.20 m to 0.40 m in the central part of the Bay of Biscay (Verdon, La Pallice, Sables d'Olonne and Saint-Nazaire; Figs. 3 and 5). These oscillations may suggest tide-surge interactions, a phenomenon which has long been known in shallow areas with large tidal ranges (Proudman, 1957; Wolf, 2009; Rego and Li, 2010; Zhang et al., 2010). Nevertheless, the period of these oscillations is of the order of 6 h while the local tide is dominated by M2, with a period of 12.42 h. In order to definitely discard the hypothesis of tide-surge interactions, a simulation was launched without tidal forcing. This simulation resulted in a surge matching very closely that of our baseline simulation, which indicates that non-linear tide-surge interactions are very weak. Pineau-Guillou et al.

(2010) performed a preliminary simulation of Xynthia surge with the HYCOM model forced by winds only and their results also display similar oscillations.

An alternative explanation for the development of such oscillations would be a resonance phenomenon, since this oscillation period of around 6 h matches the resonance period of the shelf in the central part of the Bay of Biscay (Le Cann, 1990). In order to determine the resonant mode along the Bay of Biscay, series of runs were performed forcing SELFE along the entrance of the Bay of Biscay with single tidal constituents of amplitude of 0.1 m and angular frequency varying from $0.0001 \text{ rad s}^{-1}$ to 0.001 rad s^{-1} (1.7 to 17 h period). A strong amplification (up to a factor 20) occurs in the central part of the Bay of Biscay for angular frequencies ranging from $0.00030 \text{ rad s}^{-1}$ to $0.00032 \text{ rad s}^{-1}$ (5.8–5.5 h, Fig. 12A).

As an additional verification of the role of resonance, we used the model of Clarke and Battisti (1981). Linearizing Laplace tidal equations and neglecting bottom friction, these authors proposed a simple analytical model, which suggests that resonance occurs when the following criterion is met:

$$L \approx \frac{g \cdot \alpha}{\omega^2 - f^2}, \quad (11)$$

where L is the shelf width, g is the gravity acceleration, α is the mean shelf gradient, ω is the angular frequency and f is the Coriolis parameter. The theoretical frequencies at which resonance would occur in the Bay of Biscay are shown in Fig. 12B. In the central part of the Bay of Biscay, the 140–170 km wide shelf would theoretically imply resonance for frequencies of the order of $0.0003 \text{ rad s}^{-1}$, which corroborates our numerical experiments presented in Fig. 12A. Minor discrepancies may be explained by the baseline hypotheses of Clarke and Battisti (1981), who neglected advection and bottom friction, while these two terms may be significant in the presence of islands and estuaries.

Once the resonant angular frequency ω_r is known for the central part of the Bay of Biscay, the amplitudes A_r and phases φ_r of

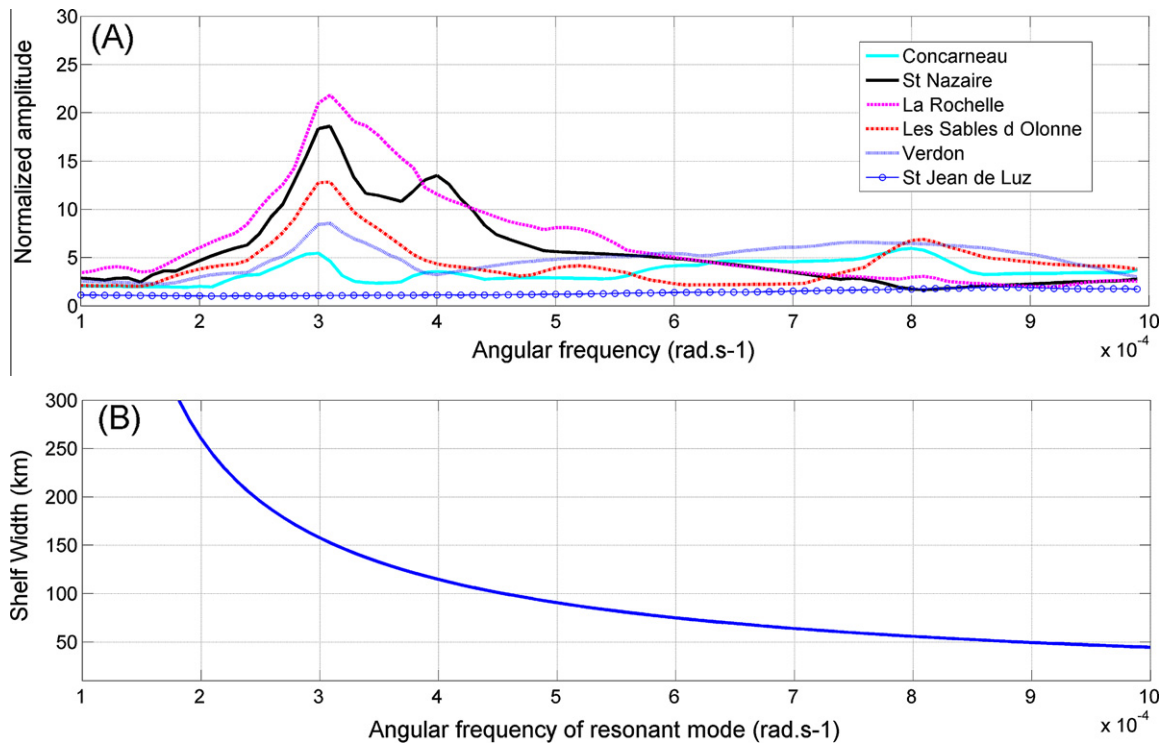


Fig. 12. A – Amplification as a function of angular frequency, showing a strong amplification in the central part of the Bay of Biscay (St Nazaire, Les Sables d'Olonne, La Pallice and Verdon) for frequencies around $0.00031 \text{ rad s}^{-1}$ (around 5.63 h). B – Shelf width at which resonance occurs as a function of angular frequency, according to the analytical model of Clarke and Battisti (1981).

the oscillations that developed in the storm surge after landfall could be estimated for each station by a least squares fit of the following equation:

$$\xi(t) = A_r \cdot \cos(\omega_r \cdot t + \varphi_r) \quad (12)$$

Predicted A_r and φ_r are compared against the values computed from observed surges (Table 3) for a 12 h period and this comparison yields an overall good agreement, with amplitude and phase discrepancies ranging from 0.02 to 0.06 m and 1–26°, respectively.

In order to illustrate the spatial repartition of this resonance phenomenon, a harmonic analysis was performed on our baseline simulation at the resonance angular frequency ω_r and over a 12 h period immediately after landfall. A contour map of the resonance oscillation amplitude is shown on Fig. 13 and reveals that the largest resonance occurred immediately to the South of landfall, where amplitudes exceed 0.2 m (0.4 m height). Resonance decreases further southward, although amplitudes increase locally in the Pertuis

Table 3

Amplitude A_r (m) and phases φ_r (°) of the resonant oscillation observed after landfall computed by means of a least square fit procedure applied to observed and modeled surge.

		Saint-Nazaire	Les Sables d'Olonne	La Pallice	Verdon
Data	A_r (m)	0.18	/	0.23	0.12
	φ_r (°)	322	/	23	8
Model	A_r (m)	0.16	0.11	0.17	0.10
	φ_r (°)	298	345	357	9

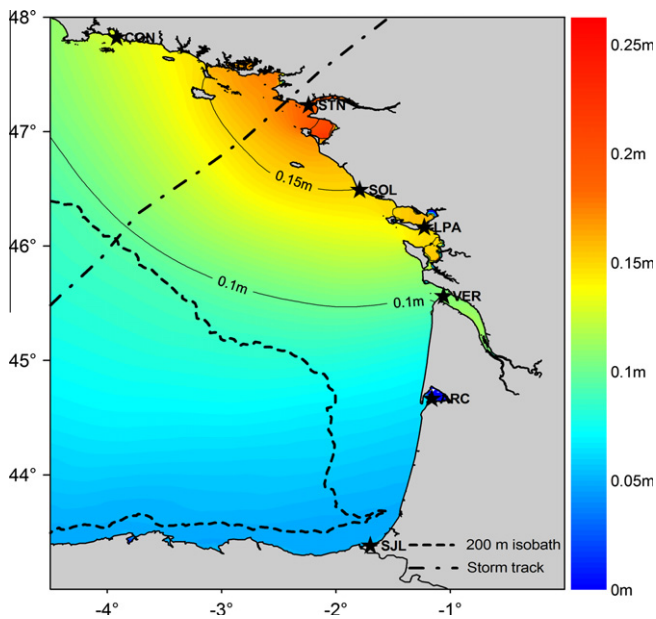


Fig. 13. Contour map of the amplitude of resonance oscillations computed at the angular frequency $\omega_r = 0.00031 \text{ rad s}^{-1}$. The dashed line indicates the 200-m isobath line and corresponds to the border of the continental shelf.

Table 4

Peak surge and amplitude of the resonant oscillation as a function of the forward speed of Xynthia at Saint-Nazaire, Les Sables d'Olonne, La Pallice and Verdon.

	Saint-Nazaire		Les Sables d'Olonne		La Pallice		Verdon	
	Peak surge (m)	A_r (m)	Peak surge (m)	A_r (m)	Peak surge (m)	A_r (m)	Peak surge (m)	A_r (m)
$v_x = 25 \text{ m/s}$ ($V_{x0} * 1.5$)	1.07	0.24	1.39	0.15	1.77	0.40	0.144	0.11
$v_x = 17 \text{ m/s}$ (V_{x0})	0.99	0.13	1.21	0.11	1.52	0.16	1.30	0.10
$v_x = 11 \text{ m/s}$ ($V_{x0}/1.5$)	1.02	0.11	1.23	0.10	1.50	0.12	1.33	0.10

Charentais and reach 0.17 m at La Pallice (Fig. 13). Depending on the station considered, this resonance oscillation represents between 10% and 25% of the total measured surge.

Several studies investigate theoretically resonance phenomena associated with storm surges, usually starting from the linearized SWE (Proudman, 1953; Nielsen et al., 2008; Vennell, 2010). In particular, Proudman (1953) showed that resonance would occur if the atmospheric disturbance travels at the same speed as the surge wave, that is \sqrt{gh} . Since Xynthia travelled the continental shelf of the Bay of Biscay at a speed of the order of $V_{x0} = 17 \text{ m s}^{-1}$, this criterion would only be met in depths of the order of 30 m. In order to investigate in further details the possible contribution of a Proudman resonance in the storm surge associated with Xynthia, numerical experiments were performed turning off tides and varying the forward speed of Xynthia from 11 to 25 m s^{-1} ($V_{x0}/1.5$ and $V_{x0} * 1.5$, respectively), through the distortion of the time in the atmospheric forcing. The results of these tests are synthesized in Table 4 and show that a slower storm drives a similar maximum surge while a faster storm drives a 10–15% larger surge peak. Such results are in agreement with those obtained in the Gulf of Mexico (Irish et al., 2008; Rego and Li, 2009) and suggest that Proudman resonance has a limited contribution in the whole storm surge.

For the three tests performed, $\sim 6 \text{ h}$ oscillations develop at the coast and their amplitude was computed using Eq. (12). Surprisingly, increasing the forward speed of Xynthia increases spectacularly the amplitude of the oscillations A_r that develop after landfall. To explain this phenomenon, spectral analyses were carried out on time-series of elevation at a point located on the track of Xynthia at the shelf break (4.20°W; 46.30°N). The analyses were performed on a 12 h window centered on the surge peak at this site, which avoids analyzing possible reflected resonant waves. This analysis shows that for the case $V_x = 25 \text{ m s}^{-1}$, about two to three times more spectral energy is found around the resonant frequency ω_r than for the baseline case, while for the case $V_x = 11 \text{ m s}^{-1}$, slightly less energy is found at this frequency. Thus, a good agreement is observed between the energy at the shelf break around the resonant frequency ω_r and the amplitude of the oscillations at the coast. This agreement demonstrates that the oscillations observed at the coast originate from the amplification of the incident storm surge energy spectrum for frequencies corresponding to the resonant mode of the shelf.

A few studies already investigated similar resonant phenomena (Moon et al., 2003), as water level anomalies published in several studies display similar oscillations. For instance, in Kennedy et al. (2011), the water level anomaly at the border between Louisiana and Texas (Gulf of Mexico) displays $\sim 12 \text{ h}$ oscillations while the wide shelf in this region causes the resonance frequency to be close to that of M2 (Reid and Whitaker, 1981). As a consequence, interactions between storm surge and continental shelf is a phenomenon expected to be relevant at other places along the world's coastlines.

7. Conclusions and future works

A new storm surge modeling system coupling the unstructured-grid circulation model SELFE (Zhang and Baptista, 2008) and the

spectral wave model WaveWatch III (Tolman, 2009) was developed to hindcast and analyze the storm surge associated with Xynthia. This modeling system was implemented over the North East Atlantic Ocean and resulted in tidal and wave predictions with scatter indexes in the Bay of Biscay of the order of 3% and 15%, respectively. The storm surge associated with Xynthia was also well predicted along the Bay of Biscay, with only a slight underestimation of the surge peak by 3–8%. Numerical experiments were then performed to screen the physical processes responsible for the storm surge development and revealed firstly that the wind drove the main part of water level anomaly through an Ekman setup process related to the S–SW orientation of storm winds. The comparison between a wave-dependant and a quadratic parameterization to compute wind stress showed that the storm surge was strongly amplified by the presence of very steep ($H_s = 7$ m vs $T_p = 7$ – 10 s) and young wind-waves, related to their rapid development in a restricted fetch. This restricted fetch resulted from the unusual track of Xynthia that crossed the Bay of Biscay from SW to NE. This result highlights the necessity of storm surge modeling systems to include a wave-dependant drag parameterization and to be able to predict accurately young sea-states, which are more challenging to model. The development of ~ 6 h oscillations observed in water level anomalies after landfall was explained by a resonant process, caused by interactions between the incident sea-level anomaly and the continental shelf in the central part of the Bay of Biscay. Such oscillations are commonly visible in previously published studies so that this resonant process is expected to be relevant at other places along the world's coastlines.

This study corresponds to the first step of an integrated research project, which aims to hindcast and analyze the storm surge and coastal flooding associated with Xynthia. Further development of our modeling system will concern the inclusion of wave radiation stress gradients, wave-induced bottom stress and the effect of currents on wave propagation and a much finer resolution will be employed to represent these processes adequately. These future improvements are expected to suppress the slight negative bias in our storm surge predictions. The numerical simulation of coastal flooding will imply using a spatial resolution locally reaching 10 m or less to represent adequately natural barrier and seawalls. Such a fine resolution would result in a computational grid with more than 10^6 nodes and the subsequent very large computational cost will be overweighed using massive parallel techniques. The representation of flooded areas will benefit from a high resolution survey, carried out a few months after Xynthia and under processing in our team. These future works are expected to allow for a deeper analysis of the flooding associated with Xynthia and a better anticipation of future risks in a context of sea-level rise and increase in storminess.

Acknowledgments

Elevation data used for model validation and storm surge characterization originated from the data bases of SONEL (www.sonel.org) and BODC (www.bodc.ac.uk/). The authors greatly thank the developing teams of the models SELFE and WaveWatchIII for making their source codes available. Wave data Offshore Oléron Island were provided by the French Oceanographic and Hydrographic Institute (SHOM) and this data was acquired during the projects MOUTON (funded by DGA PEA 012401) and EPIGRAM (funded by LEFE/IDAO and ANR, agreement ANR-08-BLAN-0330-01). Atmospheric forcing in the Bay of Biscay and the English Channel were provided by Météo France. Coarser atmospheric forcing for the whole modeled domain originated from GFS model, developed at the US National Center for Environmental Predictions. Nicolas Bruneau benefited from an invited researcher grant funded by Région Poitou-Charente. This work was partially funded by a

post-doctoral research grant to the second author from the Fundação para a Ciência (SFRH/BPD/67041/2009). The development of the modeling system was partially funded by the Portuguese Foundation for Science and Technology, throughout the projects “3D - MOWADI” (PTDC/ECM/103801/2008) and T “AdaptaRia” (PTDC/AAC-CLI/100953/2008). Tidal boundary conditions were kindly provided by UMR 5566 LEGOS. Finally, the comments of three anonymous reviewers improved this paper greatly.

References

- Ardhuin, F., Rasche, N., Belibassakis, K.A., 2008. Explicit wave averaged primitive equations using a generalized Lagrangian mean. *Ocean Modelling* 20, 35–60.
- Ardhuin, F., Chapron, B., Collard, F., 2009. Observation of swell dissipation across oceans. *Geophysical Research Letter* 36, L06607. doi:10.1029/2008GL037030.
- Ardhuin, F., Rogers, E., Babanin, A.V., Filipot, J.-F., Magne, R., Roland, A., van der Westhuysen, A., Queffelecoul, P., Lefevre, J.-M., Aouf, L., Collard, F., 2010. Semi-empirical dissipation source functions for ocean waves. Part I: definition, calibration, and validation. *Journal of Physical Oceanography* 40, 1917–1941.
- Bardet, L., Duluc, C.-L., Rebour, V., L'Her, J., 2011. Regional frequency analysis of extreme storm surges along the French coast. *Natural Hazards and Earth System Sciences* 11, 1627–1639.
- Bénard, P., 2004. ALADIN-NH/AROME dynamical core: status and possible extension to IFS. In: *Proceedings of the ECMWF Seminar*. pp. 27–40.
- Bernardara, P., Andreewsky, M., Benoit, M., 2011. Application of regional frequency analysis to the estimation of extreme storm surges. *Journal of Geophysical Research* 116, C02008. doi:10.1029/2010JC006229.
- Bertin, X., Dodet, G., 2010. Variabilité du climat de houle dans le Golfe de Gascogne au cours des six dernières décennies. In: *Proceedings of XIIème Journées Nationales Génie Côtiers – Génie Civile*, 22–24 June 2010, Les Sables d'Olonne, France.
- Bertin, X., Chaumillon, E., Sottolichio, A., Pedreros, R., 2005. Tidal inlet response to sediment infilling of the associated bay and possible implications of human activities: the Marennes–Oléron Bay and Maumusson Inlet, France. *Continental Shelf Research* 25, 115–1131.
- Bertin, X., Oliveira, A., Fortunato, A.B., 2009a. Simulating morphodynamics with unstructured grids: description and validation of a modeling system for coastal applications. *Ocean Modelling* 28 (1–3), 75–87.
- Bertin, X., Fortunato, A.B., Oliveira, A., 2009b. A modeling-based analysis of processes driving wave-dominated inlets. *Continental Shelf Research* 29, 819–834.
- Bidlot, J.-R., 2008. Intercomparison of operational wave forecasting systems against buoys: data from ECMWF, MetOffice, FNMOC, NCEP, DWD, BoM, SHOM and JMA, September 2008–November 2008. In: *Joint WMO-IOC Technical Commission for Oceanography and Marine Meteorology*.
- Blake, E.S., 2007. The deadliest, costliest and most intense United States tropical cyclones from 1851 to 2006 (and other frequently requested hurricane facts). *NOAA Technical Memorandum NWS TPC 5*, 43 pp.
- Brown, J.M., Wolf, J., 2009. Coupled wave and surge modelling for the eastern Irish Sea and implications for model wind-stress. *Continental Shelf Research* 29 (10), 1329–1342.
- Brown, J.M., Souza, A.J., Wolf, J., 2010. An 11-year validation of wave-surge modelling in the Irish Sea, using a nested POLCOMS-WAM modelling system. *Ocean Modelling* 33(1–2), 118–128.
- Brown, J., Bolanos-Sanchez, M., Rodolfo, X.X., Wolf, J., 2011. Impact assessment of advanced coupling features in a tide–surge–wave model, POLCOMS-WAM, in a shallow water application. *Journal of Marine Systems* 87(1), 13–24.
- Bruneau, N., Dodet, G., Bertin, X. and Fortunato, A. B., 2011. Development of a three-dimensional coupled wave-current model for coastal environments. *Journal of Coastal Research*, SI 64 (Proceedings of the 11th International Coastal Symposium), pp. 986–990. Szczecin, Poland, ISSN 0749-0208.
- Bunya, S., Dietrich, J.C., Westerink, J.J., Ebersole, B.A., Smith, J.M., Atkinson, J.H., et al., 2010. A high resolution coupled riverine flow, tide, wind, wind wave and storm surge model for southern Louisiana and Mississippi: Part I – model development and validation. *Monthly Weather Review* 138, 345–377.
- Butel, R., Dupuis, H., Bonneton, P., 2002. Spatial variability of wave conditions on the French Atlantic coast using in situ data. *Journal of Coastal Research* 36 (SI), 96–108.
- Chalikov, D.V., 1995. The parameterization of the wave boundary layer. *Journal of Physical Oceanography* 25, 1333–1349.
- Chalikov, D.V., Belevich, M.Yu., 1993. One-dimensional theory of the wave boundary layer. *Boundary-Layer Meteorology* 63 (1–2), 65–96. doi:10.1007/BF00705377.
- Clarke, A.J., Battisti, D.S., 1981. The effect of continental shelves on tides. *Deep-Sea Research* 28, 665–682.
- Comblen, R., Legrand, S., Deleersnijder, E., Legat, V., 2009. A finite element method for solving the shallow water equations on the sphere. *Ocean Modelling* 28 (1–3), 12–23.
- Das, P.K., 1972. A prediction model for storm surges in the Bay of Bengal. *Nature* 239, 211–213.
- Dietrich, J.C., Bunya, S., Westerink, J.J., Ebersole, B.A., Smith, J.M., Atkinson, J.H., et al., 2010. A high resolution coupled riverine flow, tide, wind, wind wave and storm surge model for southern Louisiana and Mississippi: part II – synoptic

- description and analyses of Hurricanes Katrina and Rita. *Monthly Weather Review* 138, 378–404.
- Dietrich, J.C., Zijlema, M., Westerink, J.J., Holthuijsen, L.H., Dawson, C., Luettich Jr., R.A., Jensen, R., Smith, J.M., Stelling, G.S., Stone, G.W., 2011. Modeling hurricane wave and storm surge using integrally coupled, scalable computations. *Coastal Engineering* 58, 45–65.
- Dodet, G., Bertin, X., Taborda, R., 2010. Wave climate variability in the North-East Atlantic Ocean over the last six decades. *Ocean Modelling* 31 (3–4), 120–131.
- Doodson, A.T., 1924. Meteorological perturbations of sea-level and tides. *Geophysical Journal International* 1, 124–147.
- Dupuis, H., Michel, D., Sottolichio, A., 2006. Wave climate evolution in the Bay of Biscay over two decades. *Journal of Marine Systems* 63, 105–114.
- Environmental Modeling Center, 2003. The GFS atmospheric model. NCEP Office Note 442.
- Flather, R.A., 2001. Storm surges. In: Steele, J., Thorpe, S., Turekian, K. (Eds.), *Encyclopaedia of Ocean Sciences*. Academic, San Diego, California, pp. 2882–2892.
- Fortunato, A.B., Bruneau, N., Azevedo, A., Araújo, M.A.V.C. and Oliveira, A., 2011. Automatic improvement of unstructured grids for coastal simulations. *Journal of Coastal Research*, SI 64 (Proceedings of the 11th International Coastal Symposium), pp. 1028–1032. Szczecin, Poland, ISSN 0749-0208.
- Gerritsen, H., 2005. What happened in 1953? The big flood in the Netherlands in retrospect. *Philosophical Transactions of the Royal Society A: Mathematical, Physical and Engineering Sciences* 363, 1271–1291.
- Hasselmann, K., 1974. On the spectral dissipation of ocean waves due to Whiting. *Boundary-Layer Meteorology* 6 (1–2), 107–127.
- IPCC, 2007. Climate change 2007: impacts, adaptation and vulnerability, Working Group I Report, The Physical Science Basis, Chapter 10, Global Climate projection, World Meteorological Organization, Genève, 2007, pp. 812–822.
- Irish, J.L., Resio, D.T., Ratcliff, J.J., 2008. The influence of storm size on hurricane surge. *Journal of Physical Oceanography* 38, 2003–2013.
- Janssen, P.A.E.M., 1989. Wind-induced stress and the drag of air flow over sea waves. *Journal of Physical Oceanography* 19, 745–754.
- Jelesnianski, C.P., 1965. Numerical calculation of storm tides induced by a tropical storm impinging on a continental shelf. *Monthly Weather Review* 93, 343–358.
- Jelesnianski, C.P., 1966. Numerical computations of storm surges without bottom stress. *Monthly Weather Review* 94 (6), 379–394.
- Jones, J.E., Davies, A.M., 2007. Influence of non-linear effects upon surge elevations along the west coast of Britain. *Ocean Dynamics* 57 (4–5), 401–416.
- Kennedy, A.B., Gravois, U., Zachry, B.C., Westerink, J.J., Hope, M.E., Dietrich, J.C., Powell, M.D., Cox, A.T., Luettich Jr., R.A., Dean, R.G., 2011. Origin of the Hurricane Ike forerunner surge. *Geophysical Research Letter* 28 (8), L08608.
- Le Cann, B., 1990. Barotropic tidal dynamics of the Bay of Biscay shelf: observations, numerical modelling and physical interpretation. *Continental Shelf Research* 10 (8), 723–758.
- Leffler, K.E., Jay, D.A., 2009. Enhancing tidal harmonic analysis: Robust (hybrid L1/L2) solutions. *Continental Shelf Research* 29 (1), 78–88.
- Liu, H., Xie, L., 2009. A numerical study on the effects of wave-current-surge interactions on the height and propagation of sea surface waves in Charleston Harbor during Hurricane Hugo 1989. *Continental Shelf Research* 29, 1454–1463.
- Liu, W.-C., Chen, W.-B., Hsu, M.-H., 2011. Using a three-dimensional particle-tracking model to estimate the residence time and age of water in a tidal estuary. *Computers and Geosciences* 37 (8), 1148–1161.
- Longuet-Higgins, M.S., Stewart, R.W., 1964. Radiation stresses in water waves; physical discussion, with applications. *Deep-Sea Research* 11, 529–562.
- Mastenbroek, C., Burgers, G., Janssen, P.A.E.M., 1993. The dynamical coupling of a wave model and a storm surge model through the Atmospheric Boundary Layer. *Journal of physical Oceanography* 23, 1856–1866.
- Mellor, G.L., 2008. The depth-dependent current and wave interaction equations: a revision. *Journal of Physical Oceanography* 38, 2587–2596.
- Miyazaki, M., 1965. A numerical computation of the storm surge of Hurricane Carla, 1961, in the Gulf of Mexico. *Oceanography Magazine* 17 (1–2), 109–140.
- Miyazaki, M., Okada, M., 1975. Numerical simulation of storm surges in tosa bay. *Papers in Meteorology and Geophysics* 26, 55–62.
- Moon, I.J., 2005. Impact of a coupled ocean wave-tide-circulation system on coastal modelling. *Ocean Modelling* 8, 203–236.
- Moon, I.J., Oh, I.S., Murphy, T., Youn, Y.H., 2003. Causes of the unusual coastal flooding generated by typhoon winnie on the West Coast of Korea. *Natural Hazard* 29, 485–500.
- Nicolle, A., Karpytchev, M., Benoit M., 2009. Amplification of the storm surges in shallow waters of the Pertuis Charentais (Bay of Biscay, France). *Ocean Dynamics*. doi:10.1007/s10236-009-0219-0.
- Nielsen, P., de Brye, S., Callaghan, D.P., Guard, P.A., 2008. Transient dynamics of storm surges and other forced long waves. *Coastal Engineering* 55, 499–505.
- Pairaud, I.L., Lyard, F., Auclair, F., Letellier, T., Marsaleix, P., 2008. Dynamics of the semi-diurnal and quarter-diurnal internal tides in the Bay of Biscay. Part 1: barotropic tides. *Continental shelf Research* 28, 1294–1315. doi:10.1016/j.csr.2008.03.004.
- Pineau-Guillou, L., Lathuilière, C., Magne, R., Louazel, S., Corman, D. and Perherin, C., 2010. Caractérisation des niveaux marins et modélisation des surcotes pendant la tempête Xynthia. In: Proceedings of the 11th Journées Nationales Génie Côtier-Génie Civil, Paralia ed., Les Sables d'Olonne, 22–25th of June 2010. pp. 625–634.
- Poirier, C., Sauriau, P.G., Chaumillon, E., Bertin, X., 2010. Influence of sediment dynamics on mollusc death assemblages in a temperate tide-and-wave dominated coastal environment: implications for the fossil record. *Continental Shelf Research* 30 (17), 1876–1890.
- Proudman, J., 1953. *Dynamical Oceanography*. J. Wiley, New York, p. 409.
- Proudman, J., 1957. Oscillations of tides and surge in an estuary of finite length. *Journal of Fluid Mechanics* 2, 371–382.
- Rego, J.L., Li, C., 2009. On the importance of the forward speed of hurricanes in storm surge forecasting: a numerical study. *Geophysical Research Letter* 36, L07609.
- Rego, J.L., Li, C., 2010. Nonlinear terms in storm surge predictions: effect of tide and shelf geometry with case study from Hurricane Rita. *Journal of Geophysical Research* 115, C06020.
- Reid, R.O., Whitaker, R.E., 1981. Numerical Model for Astronomical Tides in the Gulf of Mexico, Theory and Application, vol. 1. Coastal Eng. Res. Cent., U.S. Army Eng., Vicksburg, Miss., USA.
- Rodrigues, M., Oliveira, A., Guerreiro, M., Fortunato, A.B., Menaia, J., David, L.M., Cravo, A., 2011. Modeling fecal contamination in the Aljezur coastal stream (Portugal). *Ocean Dynamics* 61 (6), 841–856.
- Shen, J., Gong, W., 2009. Influence of model domain size, wind directions and Ekman transport on storm surge development inside the Chesapeake Bay: a case study of extratropical cyclone Ernesto. *Journal of Marine Systems* 75, 198–215.
- Sheng, Y.P., Zhang, Y., Paramygin, V.A., 2010. Simulation of storm surge, wave, and coastal inundation in the Northeastern Gulf of Mexico region during Hurricane Ivan in 2004. *Ocean Modelling* 35 (4), 314–331.
- Simmons, A., Uppala, S., Dee, D., Kobayashi, S., 2006. ERAInterim: new ECMWF reanalysis products from 1989 onwards. *ECMWF Newsletter* 110, 25–35.
- Simon, B., 2008. Statistiques des niveaux marins extrêmes de pleine mer en Manche et Atlantique. CD-Rom, edited by SHOM and CETMEF (in French).
- Tolman H. L., 2009. User manual and system documentation of WAVEWATCH III version 3.14. NOAA/NWS/NCEP/MMAB Technical Note 276, 194 p.
- Tolman, H.L., Chalikov, D., 1996. Source terms in a third-generation wind wave model. *Journal of Physical Oceanography* 26 (11), 2497–2518.
- Vennell, R., 2010. Resonance and trapping of topographic transient ocean waves generated by a moving atmospheric disturbance. *Journal of Fluid Mechanics* 650, 427–442.
- Weisberg, R.H., Zheng, L., 2006. A simulation of the Hurricane Charley storm surge and its breach of North Captiva Island. *Florida Scientist* 69, 152–165.
- Wolf, J., 1981. Surge-tide interaction in the North Sea and River Thames. In: Peregrine, D.H. (Ed.), *Floods Due to High Winds and Tides*. Academic press, London, pp. 75–94.
- Wolf, J., 2009. Coastal flooding: impacts of coupled wave-surge-tide models. *Natural Hazards* 49, 241–260.
- Wolf, J., Flather, R.A., 2005. Modelling waves and surges during the 1953 storm. *Philosophical transactions of the royal society A: mathematical, Physical and Engineering Sciences* 363, 1359–1375.
- Xie, L., Liu, H., Peng, M., 2008. The effect of wave-current interactions on the storm surge and inundation in Charleston Harbor during Hurricane Hugo 1989. *Ocean Modelling* 20 (3), 252–269.
- Zeng, X., Zhao, M., Dickinson, R.E., 1998. Intercomparison of bulk aerodynamic algorithms for the computation of sea surface fluxes using TOGA COARE and TAO data. *Journal of Climate* 11, 2628–2644.
- Zhang, Y.L., Baptista, A.M., 2008. SELFE: a semi-implicit Eulerian-Lagrangian finite-element model for cross-scale ocean circulation. *Ocean Modelling* 21 (3–4), 71–96.
- Zhang, M.Y., Li, Y.S., 1996. The synchronous coupling of a third-generation wave model and a two-dimensional storm surge model.
- Zhang, W.Z., Shi, F., Hong, H.S., Shang, S.-P., Kirby, J.T., 2010. Tide surge interaction intensified by the Taiwan strait. *Journal of Geophysical Research* 115, C06012. doi:10.1029/2009JC005762.
- Zhang, Y., Witter, R.W., Priest, G.P., 2011. Nonlinear tsunami-tide interaction in 1964 prince william sound tsunami. *Ocean Modelling* 40 (3–4), 246–259.